



# The role of the dual grid in low-order compatible numerical schemes on general meshes



Silvano Pitassi<sup>a,\*</sup>, Riccardo Ghiloni<sup>b</sup>, Francesco Trevisan<sup>a</sup>, Ruben Specogna<sup>a</sup>

<sup>a</sup> University of Udine, Polytechnic Department of Engineering and Architecture, EMCLab, via delle scienze 206, 33100 Udine, Italy

<sup>b</sup> University of Trento, Mathematics Department, via Sommarive 14, 38123 Povo-Trento, Italy

## ARTICLE INFO

### Article history:

Available online 17 March 2021

### Keywords:

Compatible discretizations  
Dual grid  
Polyhedral meshes  
Mimetic reconstruction  
Geometrically-defined mass matrices  
Primal and dual conservations

## ABSTRACT

In this work, we uncover hidden geometric aspect of low-order compatible numerical schemes. First, we rewrite standard mimetic reconstruction operators defined by Stokes theorem using geometric elements of the barycentric dual grid, providing the equivalence between mimetic numerical schemes and discrete geometric approaches. Second, we introduce a novel global property of the reconstruction operators, called  $P_0$ -consistency, which extends the standard consistency requirement of the mimetic framework. This concept characterizes the whole class of reconstruction operators that can be used to construct a global mass matrix in such a way that a global patch test is passed. Given the geometric description of the scheme, we can set up a correspondence between entries of reconstruction operators and geometric elements of a secondary grid, which is built by duality from the primary grid used in the scheme formulation. Finally, we show that the geometric interpretation is necessary for the correct evaluation of certain physical variables in the post-processing stage. A discussion on how the geometric viewpoint allows to optimize reconstruction operators completes the exposition.

© 2021 Elsevier Inc. All rights reserved.

## 1. Introduction

Compatible numerical schemes are designed to preserve the fundamental properties of physical and mathematical models, such as conservation laws, at the discrete level. To this end, methods of algebraic topology and differential geometry play a fundamental role. All the discrete structures necessary to develop a compatible discrete framework are put together by three basic ingredients.

To begin with, a choice of discrete representation of scalar and vector fields on a given polyhedral mesh is necessary, and is given by arrays of *degrees of freedom* (DoFs) [1]. These DoFs are defined through the *projection map* (or de Rham map [2]), i.e. the integration of the fields on specific geometric elements, where their geometric localization results from the physical nature of the fields [1], [3]. An array of DoFs has a counterpart notion in algebraic topology [4], called *cochain* [1].

Next, *discrete differential operators* acting on degrees of freedom are required. These are obtained by mimicking the fundamental theorem of calculus, namely the Stokes theorem, and they result in topological operators, as they are defined through *incidence matrices* of the grid [1], [5], [3]. This has a counterpart in concepts of algebraic topology, being the incidence matrices a matrix representation of the coboundary operator [4]. So, the coboundary operator is the discrete analogue of the gradient, curl and divergence operators [1].

\* Corresponding author.

E-mail addresses: [pitassi.silvano@spes.uniud.it](mailto:pitassi.silvano@spes.uniud.it) (S. Pitassi), [francesco.trevisan@uniud.it](mailto:francesco.trevisan@uniud.it) (F. Trevisan), [ruben.specogna@uniud.it](mailto:ruben.specogna@uniud.it) (R. Specogna).

Finally, *reconstruction operators* remap degrees of freedom back to continuous vector-valued functions, thus providing a left inverse of the projection map. The composition of the projection operator with the corresponding reconstruction map provides an interpolation operator. A reconstruction operator is said to be of *low-order* when the action of this interpolation operator leaves fixed cell-wise constant vector fields.

In this paper we focus on low-order methods for various reasons. First of all, most real three-dimensional problems are large and their exact solutions are hardly ever smooth. In these cases, low-order methods are often preferred in order to reduce the number of unknowns. Moreover, high order schemes suffer from the lack of high order representation of curved geometry in off-the-shelf mesh generators. Finally, physical and geometric parameters are generally known with a tolerance in the percent range, that is why extreme accuracy is unjustified in practice.

A central role played by reconstruction operators is in the construction of the *discrete Hodge operator* [2], [6], which provides a discrete inner product on the space of discrete vector fields and it is required to satisfy two properties [7], [8]. The first one is a *polynomial consistency condition*, which is an exactness property on a well-defined family of polynomials. In particular, for the low-order case we want to enforce  $P_0$ -polynomial consistency, where symbol  $P_0$  refers to exactness for constant fields (i.e. polynomials of degree 0). The second one is a *stability condition*, which ensures the well-posedness of the numerical scheme. From the practical point of view, the *patch test* can be used to test if both requirements are satisfied [9]. Both  $P_0$ -consistency and stability conditions are stated at a global level, since they are properties of the global mass matrix representing the algebraic realization of the discrete Hodge operator. However, as we will see, the global mass matrix is constructed from local mass matrices, and the latter are constructed from local reconstruction operators. Thus, the design of a global mass matrix that satisfy  $P_0$ -polynomial consistency and stability conditions must start at the local level with a suitable choice of local reconstruction operators.

A well established design strategy decomposes a local mass matrix as the sum of a *consistent* and a *stabilization* term [10], [8]. Such a decomposition of the local mass matrix is suggestive since each term plays a specific role, namely, the consistent term enforces the polynomial consistency property while the stabilization term ensures positive-definiteness, preserving the consistency already achieved. Since the building blocks of local mass matrices are reconstruction operators, a similar decomposition can be equivalently performed on reconstruction operators [11].

We can identify two main approaches to design low-order compatible numerical schemes. The first approach relies on a primal-dual grid structure and the related staggered positioning of the discrete variables. In this category fall most physics-compatible discretizations introduced so far, like the Discrete Geometric Approach (DGA) [12], [13], [14], cell method (CM) [15], [5], [16], generalized finite differences [17] as well as in Compatible Discrete Operators (CDO) [18], [19], [11]. Once a dual grid structure is assumed from the beginning as part of the numerical scheme, the consistency condition is satisfied by resorting to the so called *Bossavit's consistency criterion* [7], [17], and, as already recognized in [11], [19], reconstruction operators have a clear geometric interpretation being defined by geometric elements of the dual grid.

In other physics-compatible methods like the Mimetic Finite Difference method (MFD) [10], [8], Finite Volumes (FV) [20], reconstruction operators are defined by mimicking the continuous Stokes theorem, but without introducing at all a dual grid. This strategy of designing reconstruction operators is also employed in the high order generalization of the MFD schemes [21], and in some recent high order compatible methods [22], which include the low-order version as a limit case.

In this paper we provide new geometric viewpoints of low-order compatible numerical schemes. In particular, we uncover two main geometric aspects that are hidden in the MFD method.

As a first contribution, we show that reconstruction operators defined by mimicking the Stokes theorem, introduced in [23], lead to reconstruction operators defined by geometric elements of the barycentric dual grid. This result shows that the reconstruction operators used in the two main families of low-order compatible numerical schemes are equivalent. As a consequence, consistent terms of local mass matrices are the same and the only difference relies only on the particular choice of the stabilization term. This result extends the approach proposed in the FV literature [20] by introducing a novel reconstruction formula for edge DoFs. We point out that, although in the approach presented in [20] the reconstruction formula for face DoFs is derived, its identification with dual edges is not highlighted. The derivation of the novel edge formula completes the picture of the relation with the dual barycentric grid. Since the barycentric dual grid is already present in the scheme, although not made explicit, we present a novel geometric numerical scheme which is a hybrid approach between the MFD method and the discrete geometric formulations. Here, a barycentric dual grid is assumed as part of the numerical scheme and the stabilization technique proposed in the mimetic literature is employed. The resulting scheme benefits from all the advantages of the two methodologies: the geometric structure allows us to write balance laws explicitly and simplifies the scheme software implementation [3], while the stabilization term offers the possibility of changing properties of the local mass matrices through the selection of some user-dependent parameters. Finally, the equivalence of the consistent terms also implies that mathematical results obtained for the MFD method, such as convergence properties or error estimates, can be readily extended to this unified framework, and in general to the discrete geometric formulations.

A second contribution of this paper is to introduce a novel property of the reconstruction operators, to which we refer as  $P_0$ -consistency. As the name suggests, a set of  $P_0$ -consistent reconstruction operators is such that the global mass matrix constructed using them satisfies the  $P_0$ -consistency property. The main difference with respect to the set of requirements that characterize reconstruction operators introduced in [23] is that the new definition of  $P_0$ -consistency is a global property since it involves reconstruction operators defined on more than one cell. The formal definition of this concept is based on a commuting diagram property of the discrete de Rham complex and its dual, which lie at the foundations of the mathematical structure of physical theories, as represented graphically by Tonti diagrams [3]. This approach extends what

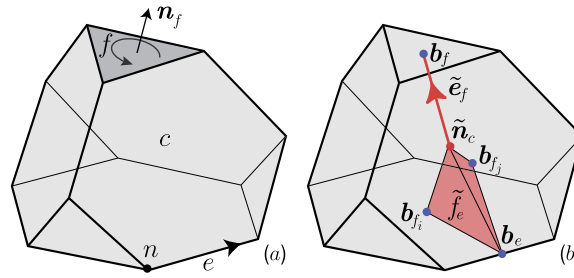


Fig. 1. (a) Primal and (b) dual geometric elements of a polyhedron  $c \in C$ .

is usually done in literature. In [11], a dual grid is introduced as part of the numerical scheme and then its relation with reconstruction operators is identified. In our approach, instead, the barycentric dual grid is derived as a canonical choice of designing  $P_0$ -consistent reconstruction operators on general polyhedral cells, and as an additional result of our analysis, it is the only possible construction if we restrict the design of reconstruction operators at the single cell level, without taking into account reconstruction operators of other cells. The fundamental role played by Stokes theorem in mimetic numerical schemes appears, therefore, as the geometric manifestation of the necessity of using the barycentric dual grid to design local reconstruction operators. A geometric characterization of  $P_0$ -consistent reconstruction operators can be given as the affine solution space of a linear system of equations, and from a physical point view, we show that it is directly connected with conservation laws of physical theories. An analysis of this linear system constitutes the starting point to geometrically optimize discrete Hodge operators. As an instance, it reveals that besides the barycentric dual grid there are other possible dual grids which are not constructed according to the barycentric subdivision. In addition, for every cell we can choose an arbitrary point in space to geometrically define the entries of local reconstruction operators. We provide an example of how this freedom of choice in the design of reconstruction operators can be used to optimize them, as measured by a  $L^2$  norm.

The paper is organized as follows. In Section 2, we introduce the geometric elements from which general polyhedral grids are constructed. In Section 3, we present the basic building blocks of low-order compatible numerical schemes. In Section 4, we describe the  $P_0$ -consistency property of reconstruction operators. In Section 5, we give proofs of the equivalence of mimetic reconstruction operators and the ones defined by geometric elements of the barycentric dual grid. In Section 6, we show examples of how this analysis can be used to design new numerical schemes. Finally, in Section 7, the conclusions are drawn.

## 2. Pair of interlocked grids and geometric properties

Let us consider a subdivision of a polyhedral region  $\Omega \subset \mathbb{R}^3$  into a primal grid  $K = (N, E, F, C)$ , where the sets  $N, E, F$  and  $C$  contain the grid nodes, edges, faces and cells, respectively. We denote a single node as  $n$ , an edge by  $e$ , a face by  $f$  and a cell by  $c$ , respectively, see Fig. 1(a). The geometric elements of the primal grid are provided with an inner orientation [1], [3].

Interlocked with the primal grid, a barycentric dual grid [4], [1], [3] is introduced; each geometric entity of the dual grid is in one-to-one correspondence (duality pairing) with a geometric element of the primal grid and it is constructed by means of the barycentric subdivision [4] of the primal grid. With symbol “ $\sim$ ” we denote geometric elements of the dual grid and with a subscript we indicate the corresponding (unique) geometric element of the primal grid. The dual of a primal cell  $c$  is the dual node denoted as  $\tilde{n}_c$ ; similarly the dual of a primal edge  $e$  is a dual face  $\tilde{f}_e$  and the dual of a primal face  $f$  is a dual edge  $\tilde{e}_f$ .

To describe the geometric elements of the pair of grids, we introduce a Cartesian system of coordinates with specified origin and we denote by  $\mathbf{x} = (x_1, x_2, x_3)^T$  the coordinates of its generic point. Let us consider, for the sake of clarity, a single cell  $c$ , as the one pictured in Fig. 1(a). The geometric construction of the dual nodes, dual edges and dual faces is based on the barycentric subdivision as follows, see Fig. 1(b). To begin with, let us define the barycenters of geometric elements. The barycenters of edge  $e$ , face  $f$  and cell  $c$  are defined, respectively, as follows

$$\mathbf{b}_e = \frac{1}{|e|} \int_e \mathbf{x} dl, \quad \mathbf{b}_f = \frac{1}{|f|} \int_f \mathbf{x} dS, \quad \mathbf{b}_c = \frac{1}{|c|} \int_c \mathbf{x} dV, \quad (1)$$

where  $|e|, |f|$  and  $|c|$  denote the length of edge  $e$ , the area of face  $f$  and the volume of cell  $c$ , respectively. In the following, we will use a generalized construction for the barycentric dual grid in which the dual node  $\tilde{n}_c$  is an arbitrary point and does not necessarily coincide with the barycenter  $\mathbf{b}_c$  of the cell  $c$ . We refer to such a construction again as barycentric dual grid, although the dual node does not coincide with the barycenter  $\mathbf{b}_c$  of the cell  $c$ . A dual edge  $\tilde{e}_f$  is a segment which joins  $\tilde{n}_c$  with the barycenter  $\mathbf{b}_f$  of a primal face  $f$ , see the construction in Fig. 1(b). A dual face  $\tilde{f}_e$  is a quadrilateral surface made of a union of a pair of triangles; the first has the vertices  $\tilde{n}_c, \mathbf{b}_e, \mathbf{b}_{f_i}$ , the second the vertices  $\tilde{n}_c, \mathbf{b}_e, \mathbf{b}_{f_j}$ , with  $f_i, f_j$  the

two primal faces having the edge  $e$  in common. Dual edge  $\tilde{e}_f$  and dual face  $\tilde{f}_e$  are endowed with outer orientation [1], [3], in such a way that each of the pairs  $(e, \tilde{f}_e)$ ,  $(f, \tilde{e}_f)$  are oriented according to the right-hand rule.

To each of the following geometric elements  $e, f, \tilde{f}, \tilde{e}$  of the primal or of the dual grid, we associate their corresponding vectors  $\mathbf{e}, \mathbf{f}, \tilde{\mathbf{f}}, \tilde{\mathbf{e}}$  respectively. Any of these vectors, will be represented with a column array of its Cartesian components. Vector  $\mathbf{e}$  is the edge vector associated with edge  $e$ ; for example  $\mathbf{e} = (e_1, e_2, e_3)^T = \mathbf{n}_i - \mathbf{n}_j$ ,  $i \neq j$ , where  $\mathbf{n}_i$  and  $\mathbf{n}_j$  are the coordinates of the boundary nodes of  $e$ .  $\mathbf{t}_e$  represents the unit vector of  $\mathbf{e}$  in such a way that  $\mathbf{e} = |\mathbf{e}|\mathbf{t}_e$ . Vector  $\mathbf{f}$  is the face vector associated with face  $f$  defined as  $\mathbf{f} = |f|\mathbf{n}_f$ , where  $\mathbf{n}_f$  is the unit normal vector orthogonal to  $f$ . In a similar way, vector  $\tilde{\mathbf{e}}_f$  is the edge vector associated with the dual edge  $\tilde{e}_f$ ; for instance,  $\tilde{\mathbf{e}}_f = \mathbf{b}_f - \tilde{\mathbf{n}}_c$ , see Fig. 1(b). Vector  $\tilde{\mathbf{f}}_e$  is the face vector associated with the dual face  $\tilde{f}_e$ . Face vector  $\tilde{\mathbf{f}}_e$  is equal to  $\tilde{\mathbf{f}}_e = \frac{1}{2}(\tilde{\mathbf{e}}_{f_i} \times (\mathbf{b}_e - \tilde{\mathbf{n}}_c) - \tilde{\mathbf{e}}_{f_j} \times (\mathbf{b}_e - \tilde{\mathbf{n}}_c))$  with  $f_i, f_j$  two faces such that  $e = f_i \cap f_j$ , with  $i = i(e)$  and  $j = j(e)$ , and in such a way that the expression induces the correct orientation on  $\tilde{\mathbf{f}}_e$ , see Fig. 1(b).

### 2.1. Degrees of freedom

We define a *discrete field* as a collection of degrees of freedom (DoFs). DoFs are arrays of real numbers whose entries are obtained by evaluating the physical scalar or vector fields on the geometric elements of the mesh by means of integration [24], [1], [7]. The operation of translating a sufficiently smooth scalar or vector-valued functions into DoFs is performed by *projection maps*, called also *de Rham maps* [2], [7].

Let  $u$  be a sufficiently regular scalar function so that we can take its pointwise values. We denote with  $S^N$  the space of such functions. For instance,  $S^N$  can be taken to be  $H^1(\Omega) \cap C^0(\Omega)$ . Node projection operator  $P^N$  maps  $u$  onto its node DoFs  $u^N = P^N(u)$ , where the entry of  $u^N$  corresponding to node  $n$  is

$$u_n^N = u(n). \quad (2)$$

We denote the vector space of node DoFs by  $\mathcal{N} = \mathbb{R}^{\text{card}(\mathcal{N})}$ .

Let  $\mathbf{u}$  be a sufficiently regular vector-valued function so that the integrals of its tangential components are well defined along the grid edges. We denote with  $S^E$  the space of all such functions. For instance,  $S^E$  can be taken to be  $H^s(\Omega)$ , with  $s > 1$ . Edge projection operator  $P^E$  maps  $\mathbf{u}$  onto its edge DoFs  $\mathbf{u}^E = P^E(\mathbf{u})$ , where the entry of  $\mathbf{u}^E$  corresponding to edge  $e$  is

$$\mathbf{u}_e^E = \int_e \mathbf{u} \cdot \mathbf{t}_e dl. \quad (3)$$

We denote the vector space of edge DoFs by  $\mathcal{E} = \mathbb{R}^{\text{card}(\mathcal{E})}$ .

Now, let  $\mathbf{u}$  be a sufficiently regular vector-valued function so that the integrals of its normal components are well defined on the grid faces. We denote with  $S^F$  the space of all such functions. For instance,  $S^F$  can be taken to be  $H^s(\Omega)$ , with  $s > \frac{1}{2}$ . Face projection operator  $P^F$  maps  $\mathbf{u}$  onto its face DoFs  $\mathbf{u}^F = P^F(\mathbf{u})$ , where the entry of  $\mathbf{u}^F$  corresponding to face  $f$  is

$$\mathbf{u}_f^F = \int_f \mathbf{u} \cdot \mathbf{n}_f dS. \quad (4)$$

We denote the vector space of face DoFs by  $\mathcal{F} = \mathbb{R}^{\text{card}(\mathcal{F})}$ .

Let  $u$  be a sufficiently regular scalar function so that its integrals on compact subsets of  $\Omega$  are well-defined. We denote with  $S^C$  the space of such functions. For instance,  $S^C$  can be taken to be  $L^1(\Omega)$ . Cell projection operator  $P^C$  maps  $u$  onto its cell DoFs  $u^C = P^C(u)$ , where the entry of  $u^C$  corresponding to cell  $c$  is

$$u_c^C = \int_c u dV. \quad (5)$$

We denote the vector space of cell DoFs by  $\mathcal{C} = \mathbb{R}^{\text{card}(\mathcal{C})}$ .

Let  $\mathcal{X}$  be any set among  $\mathcal{N}, \mathcal{E}, \mathcal{F}$  or  $\mathcal{C}$ . For a given cell  $c$ , we denote with  $\mathcal{X}_c$  the vector subspace of all DoFs of  $\mathcal{X}$  that are attached to geometric elements of cell  $c$ . Then, the *local projection operator* on cell  $c$  is defined as  $P_c^{\mathcal{X}}: S_c^{\mathcal{X}} \rightarrow \mathcal{X}_c$ , where  $S_c^{\mathcal{X}}$  is finite dimensional vector subspace of  $S^{\mathcal{X}}$  chosen in such a way that the map  $P_c^{\mathcal{X}}$  is bijective on  $\mathcal{X}_c$ . Thus, we can set up a correspondence between a vector field  $\mathbf{u} \in S_c^{\mathcal{X}}$  and its corresponding DoFs. We point out that in the following we do not need to construct explicitly the space  $S_c^{\mathcal{X}}$  since only its generic properties will be used.

Let  $\mathbb{P}_c^{\mathcal{X}}$  be the matrix associated with the restriction of the map  $P_c^{\mathcal{X}}: S_c^{\mathcal{X}} \rightarrow \mathcal{X}_c$  to the vector subspace of *constant* scalar or vector fields. Specifically, rows of  $\mathbb{P}_c^{\mathcal{E}}$  and  $\mathbb{P}_c^{\mathcal{F}}$  collect the coefficients with respect to the standard base of  $\mathbb{R}^3$  of the quantities  $\int_e \mathbf{t}_e dl$  and  $\int_f \mathbf{n}_f dS$ , respectively. Given a constant vector field  $\mathbf{u}$  defined on  $c$ , by Stokes theorem, the latter integral quantities can also be computed on any homologous geometric element. In particular, matrices  $\mathbb{P}_c^{\mathcal{E}}$  and  $\mathbb{P}_c^{\mathcal{F}}$  can be written as

$$\mathbb{P}_c^{\mathcal{F}} = \begin{pmatrix} \vdots \\ \mathbf{f}_i^T \\ \vdots \end{pmatrix}, \quad \mathbb{P}_c^{\mathcal{E}} = \begin{pmatrix} \vdots \\ \mathbf{e}_i^T \\ \vdots \end{pmatrix}. \tag{6}$$

In what follows, we will also need the dual counterpart of matrices  $\mathbb{P}^{\mathcal{E}}, \mathbb{P}^{\mathcal{F}}$ . We denote by  $\mathbb{P}_{\tilde{\mathbf{n}}_c}^{\tilde{\mathcal{E}}}$  the matrix whose rows collect dual edge vectors  $\tilde{\mathbf{e}}_f$  of  $c$ , constructed using the dual node  $\tilde{\mathbf{n}}_c$ . For the special case where  $\tilde{\mathbf{n}}_c$  coincides with the origin we use the symbol  $\mathbb{P}_c^{\tilde{\mathcal{E}}}$ . In a similar way, we denote with  $\mathbb{P}_{\tilde{\mathbf{n}}_c}^{\tilde{\mathcal{F}}}$  the matrix whose rows collect dual face vectors  $\tilde{\mathbf{f}}_e$  of  $c$ , constructed using the dual node  $\tilde{\mathbf{n}}_c$ . For the special case where  $\tilde{\mathbf{n}}_c$  coincides with the origin we use the symbol  $\mathbb{P}_c^{\tilde{\mathcal{F}}}$ .

### 3. Compatible numerical schemes

In this section we introduce the main ingredients which lie at the foundations of any compatible numerical scheme. Specialized definitions are given for the low-order case.

#### 3.1. Discrete differential operators

One kind of equation that we find in physical theories are *balance equations* [1], [3]. A differential operator usually arises in the continuous form of balance equations and thus, in numerical schemes we need its discrete counterpart. Stokes theorem provides discrete counterparts of the differential operators gradient, curl and divergence [24], [1], [5]. Discrete differential operators can be defined for both the primal and the dual grid and they are defined in matrix form by incidence matrices of the pair of grids [1]. An entry of each of these matrices corresponding to a given pair of oriented geometric elements of the primal grid is equal to 0, if the two geometric elements are not mutually incident, otherwise, 1 if their mutual orientations are compatible and  $-1$  if not [3].

From their definition discrete differential operators encode the topology of problem: being metric free, any stretching or deformation of the mesh does not change their form.

The *discrete gradient operator* maps any node DoFs in  $\mathcal{N}$  into edge DoFs in  $\mathcal{E}$ , and is defined through the action of a matrix

$$\mathcal{GRAD} := \mathbb{G} \mathbf{u}^{\mathcal{N}}, \tag{7}$$

where  $\mathbb{G}$  is the  $\text{card}(\mathcal{E}) \times \text{card}(\mathcal{N})$ -matrix of incidence numbers between nodes and edges.

The *discrete curl operator* maps any edge DoFs in  $\mathcal{E}$  into face DoFs in  $\mathcal{F}$ , and is defined through the action of a matrix

$$\mathcal{CURL}(\mathbf{u}^{\mathcal{E}}) := \mathbb{C} \mathbf{u}^{\mathcal{E}}, \tag{8}$$

where  $\mathbb{C}$  is the  $\text{card}(\mathcal{F}) \times \text{card}(\mathcal{E})$ -matrix of incidence numbers between edges and faces.

The *discrete divergence operator* maps any face DoFs in  $\mathcal{F}$  into cell DoFs in  $\mathcal{C}$ , and is defined through the action of a matrix

$$\mathcal{DIV}(\mathbf{u}^{\mathcal{F}}) := \mathbb{D} \mathbf{u}^{\mathcal{F}}, \tag{9}$$

where  $\mathbb{D}$  is the  $\text{card}(\mathcal{C}) \times \text{card}(\mathcal{F})$ -matrix of incidence numbers between faces and cells.

#### 3.2. Reconstruction operators

*Reconstruction operators* are designed to remap DoFs into the corresponding continuous vector field. In contrast to the projection operator, where the de Rham map is the obvious candidate, the choice of the reconstruction operator is flexible because there are many possible ways in which global physical quantities can be combined to a local field representation.

Let  $R_c^{\mathcal{X}} : \mathcal{X}_c \rightarrow S_c^{\mathcal{X}}$  be the reconstruction operator from the vector space  $\mathcal{X}_c$  of DoFs restricted to cell  $c$ . In [8], reconstruction operators are required to satisfy a number of formal properties that involve the projection operator and the continuous and discrete differential operators. However, for the low-order case, from this set of properties it is sufficient to require that reconstruction operators satisfy only the so called *accuracy property* [8]:  $R_c^{\mathcal{X}}$  is a left inverse of  $P_c^{\mathcal{X}}$ , i.e.

$$(R_c^{\mathcal{X}} \circ P_c^{\mathcal{X}})(\mathbf{u}) = \mathbf{u}, \quad \forall \mathbf{u} \in S_c^{\mathcal{X}}. \tag{10}$$

As we will see, since we are interested in the low-order case, we never need an explicit expression of the reconstruction operator, but only its averaged quantities over a cell come into play. To this end in mind, let us introduce the *average reconstruction operator*  $\overline{R}_c^{\mathcal{X}} : \mathcal{X}_c \rightarrow S_c^{\mathcal{X}}$  as a map whose values are constant vector fields in  $c$ , defined as follows

$$\overline{R}_c^{\mathcal{X}}(\mathbf{u}_c^{\mathcal{X}}) := \frac{1}{|c|} \int_c R_c^{\mathcal{X}}(\mathbf{u}_c^{\mathcal{X}}) dV, \quad \forall \mathbf{u}_c^{\mathcal{X}} \in \mathcal{X}_c. \tag{11}$$

Let  $\mathbb{R}_c^X$  be the matrix associated with the map  $\overline{R}_c^X$ . The accuracy property requires that  $\mathbb{R}_c^X$  is a left inverse of  $\mathbb{P}_c^X$ . To see this, observe that  $\overline{R}_c^X(\text{im}(\mathbb{P}_c^X)) = R_c^X(\text{im}(\mathbb{P}_c^X))$  and  $\text{im}(\mathbb{P}_c^X) \subset \mathcal{X}_c$ .

An additional property that reconstruction operators have to satisfy is the so called  $P_0$ -consistency and it will be formally defined in Section 4. Informally, these are the reconstruction operators that can be used to construct a global mass matrix, according to the recipe detailed in Section 3.3 and Section 3.4, that satisfies the  $P_0$ -consistency property.

### 3.3. Local mass matrix

Let us consider a symmetric, positive-definite  $3 \times 3$ -matrix  $\mathbb{K}_c$  representing the material property of a cell  $c$ , assumed to be homogeneous in  $c$ . We want to introduce an inner product on vector spaces  $\mathcal{N}, \mathcal{E}, \mathcal{F}$  and  $\mathcal{C}$  that is a low-order approximation of classical  $L^2$  product between two continuous vector functions  $\mathbf{u}, \mathbf{v}$

$$\langle \mathbf{u}_c^X, \mathbf{v}_c^X \rangle_{\mathcal{X},c} = \int_c \mathbf{u} \cdot (\mathbb{K}_c \mathbf{v}) dV + \mathcal{O}(h|c|), \quad \forall \mathbf{u}, \mathbf{v} \in S_c^X, \quad (12)$$

where  $h$  denotes a characteristic size of the mesh and  $\mathbf{u}_c^X, \mathbf{v}_c^X$  are the DoFs restricted to a cell  $c$  of  $\mathbf{u}, \mathbf{v}$ , respectively. The bilinear form can be expressed in matrix form through a symmetric and positive-definite matrix  $\mathbb{M}_c^X$  which acts on the local DoFs

$$\langle \mathbf{u}_c^X, \mathbf{v}_c^X \rangle_{\mathcal{X},c} = (\mathbf{u}_c^X)^T \mathbb{M}_c^X \mathbf{v}_c^X. \quad (13)$$

In view of (12), the local matrix  $\mathbb{M}_c^X$  must contain information about the material property  $\mathbb{K}_c$  on  $c$ .

We want to design  $\mathbb{M}_c^X$  in such a way that it satisfies the following three conditions [7], [17], [25], [8]:

1. symmetric;
2. positive-definite;
3. *consistency condition* [8]: if  $\mathbf{u}$  is a constant vector field and  $\mathbf{v} \in S_c^X$ , the following equality holds for every cell  $c$

$$(\mathbf{u}_c^X)^T \mathbb{M}_c^X \mathbf{v}_c^X = \int_c \mathbf{u} \cdot (\mathbb{K}_c \mathbf{v}) dV, \quad \forall \mathbf{v} \in S_c^X. \quad (14)$$

Suppose that we want to satisfy the three requirements above. Under the above assumptions, we now introduce an equivalent algebraic form of the consistency condition (14). The derivation is strictly related to the one proposed in mimetic literature, see [8].

Let  $\mathbf{u}$  be a constant vector field and let  $\mathbf{v}$  be an element of  $S_c^X$ . We can rewrite in an equivalent way the consistency condition (14) as

$$(\mathbb{P}_c^X(\mathbf{u}))^T \mathbb{M}_c^X \mathbf{v}_c^X = \int_c \mathbf{u} \cdot (\mathbb{K}_c R_c^X(\mathbf{v}_c^X)) dV, \quad \forall \mathbf{v}_c^X \in \mathcal{X}_c. \quad (15)$$

Since  $\mathbf{u}$  is constant inside  $c$ , we introduce the matrix form of the projection operator  $\mathbb{P}_c^X$ . In addition, since both  $\mathbf{u}$  and  $\mathbb{K}_c$  are constant inside the cell  $c$ , by using the definition of the matrix  $\mathbb{R}_c^X$  associated with the average reconstruction operator  $\overline{R}_c^X$  on the cell  $c$ , it follows that

$$\mathbf{u}^T (\mathbb{P}_c^X)^T \mathbb{M}_c^X \mathbf{v}_c^X = |c| \mathbf{u} \cdot (\mathbb{K}_c \mathbb{R}_c^X \mathbf{v}_c^X), \quad \forall \mathbf{v}_c^X \in \mathcal{X}_c. \quad (16)$$

The above equality must hold for every vector  $\mathbf{u}$  and DoF  $\mathbf{v}_c^X$ , thus we obtain the following condition

$$(\mathbb{P}_c^X)^T \mathbb{M}_c^X = |c| \mathbb{K}_c \mathbb{R}_c^X. \quad (17)$$

By transposing both members we can finally write

$$\mathbb{M}_c^X \mathbb{P}_c^X = |c| (\mathbb{R}_c^X)^T \mathbb{K}_c. \quad (18)$$

Condition expressed in (18) is called *algebraic consistency condition* in mimetic literature [8]. The following lemma shows that a solution of (18) can always be written as the sum of two terms, which is the canonical solution proposed in [8].

**Lemma 1.** Let  $\mathbb{K}_c$  be a symmetric and positive-definite matrix and let  $\mathbb{R}_c^X$  be a left inverse of  $\mathbb{P}_c^X$ . Let  $\alpha = (\alpha_1, \dots, \alpha_{n-3}) \in (\mathbb{R}^+)^{n-3}$  be any  $(n-3)$ -upla of positive real numbers and let  $\mathbb{D}_\alpha$  be the diagonal matrix whose diagonal entries are  $\alpha_1, \dots, \alpha_{n-3}$ . Let  $\mathbf{w} = (\mathbf{w}_1, \dots, \mathbf{w}_{n-3})$  be any orthonormal basis of  $\text{im}(\mathbb{P}_c^X)^\perp$  and let  $\mathbb{W}_{c,\mathbf{w}}$  be the matrix whose columns are the vectors  $\mathbf{w}_1, \dots, \mathbf{w}_{n-3}$ . Define  $\mathbb{M}_c^X$  by setting

$$\mathbb{M}_c^X := |c|(\mathbb{R}_c^X)^T \mathbb{K}_c \mathbb{R}_c^X + \mathbb{W}_{c,w} \mathbb{D}_\alpha \mathbb{W}_{c,w}^T$$

Then the matrix  $\mathbb{M}_c^X$  is symmetric, consistent and positive-definite.

### 3.4. Global mass matrix

For each  $c \in C$ , let  $\mathbb{S}_c^X$  be the matrix which assigns DoFs of  $c$  when it is applied to an element of  $X$ .  $\mathbb{S}_c^X$  is a matrix of size  $\dim(\mathcal{X}_c) \times \dim(X)$  and every row has exactly one entry equal to 1 corresponding to a element which is in  $c$  and zero everywhere else.

For each  $c \in C$ , let  $\mathbb{M}_c^X$  be a local mass matrix associated with  $c$  defined as in Lemma 1. With this definition, we obtain

$$(\mathbf{u}^X)^T \mathbb{M}^X \mathbf{v}^X = \sum_{c \in C} (\mathbb{S}_c^X \mathbf{u}^X)^T \mathbb{M}_c^X (\mathbb{S}_c^X \mathbf{v}^X) = (\mathbf{u}^X)^T \left( \sum_{c \in C} (\mathbb{S}_c^X)^T \mathbb{M}_c^X \mathbb{S}_c^X \right) \mathbf{v}^X, \tag{19}$$

from which follows the expression of the global mass matrix

$$\mathbb{M}^X = \sum_{c \in C} (\mathbb{S}_c^X)^T \mathbb{M}_c^X \mathbb{S}_c^X. \tag{20}$$

### 3.5. Derived discrete operators

In this subsection we recall the definition of the derived discrete operators  $\widetilde{\mathcal{GRAD}}$ ,  $\widetilde{\mathcal{CURL}}$  and  $\widetilde{\mathcal{DIV}}$  which are obtained through a duality relation from the discrete operators  $\mathcal{GRAD}$ ,  $\mathcal{CURL}$  and  $\mathcal{DIV}$ , respectively. Let us suppose that the discrete spaces  $N$ ,  $\mathcal{E}$ ,  $\mathcal{F}$  and  $C$  are equipped with inner products as detailed in Section 3.3 and Section 3.4.

Let us now define the derived operators. The adjoints of the discrete differential operators  $\mathcal{GRAD}$ ,  $\mathcal{CURL}$  and  $\mathcal{DIV}$  will be denoted by  $\mathcal{GRAD}^*$ ,  $\mathcal{CURL}^*$  and  $\mathcal{DIV}^*$ . It is convenient to rename the adjoints operators as follows  $\widetilde{\mathcal{GRAD}} \cong -\mathcal{DIV}^*$ ,  $\widetilde{\mathcal{CURL}} \cong \mathcal{CURL}^*$  and  $\widetilde{\mathcal{DIV}} \cong -\mathcal{GRAD}^*$ . By using the definition of  $\mathcal{DIV}^*$  and the identification  $\widetilde{\mathcal{GRAD}} \cong -\mathcal{DIV}^*$  we obtain

$$\langle \mathbf{u}^{\mathcal{F}}, \widetilde{\mathcal{GRAD}} p^C \rangle_{\mathcal{F}} = -\langle \mathbf{u}^{\mathcal{F}}, \mathcal{DIV}^* p^C \rangle_{\mathcal{F}} = -\langle \mathcal{DIV} \mathbf{u}^{\mathcal{F}}, p^C \rangle_C \quad \forall \mathbf{u}^{\mathcal{F}} \in \mathcal{F}, p^C \in C. \tag{21}$$

As  $\mathbf{u}^{\mathcal{F}}$  and  $p^C$  are arbitrary it follows that

$$\widetilde{\mathcal{GRAD}} \cong -\mathcal{DIV}^* = -\mathbb{M}^{\mathcal{F}-1} \mathcal{DIV}^T \mathbb{M}^C. \tag{22}$$

By using the definition of  $\mathcal{CURL}^*$  and the identification  $\widetilde{\mathcal{CURL}} \cong \mathcal{CURL}^*$  we obtain

$$\langle \mathbf{u}^{\mathcal{E}}, \widetilde{\mathcal{CURL}} \mathbf{w}^{\mathcal{F}} \rangle_{\mathcal{E}} = \langle \mathbf{u}^{\mathcal{E}}, \mathcal{CURL}^* \mathbf{w}^{\mathcal{F}} \rangle_{\mathcal{E}} = \langle \mathcal{CURL} \mathbf{u}^{\mathcal{E}}, \mathbf{w}^{\mathcal{F}} \rangle_{\mathcal{F}} \quad \forall \mathbf{u}^{\mathcal{E}} \in \mathcal{E}, \mathbf{w}^{\mathcal{F}} \in \mathcal{F} \tag{23}$$

from which we obtain that

$$\widetilde{\mathcal{CURL}} = \mathbb{M}^{\mathcal{E}-1} \mathcal{CURL}^T \mathbb{M}^{\mathcal{F}}. \tag{24}$$

Similarly, the duality relation between the discrete gradient operator  $\mathcal{GRAD}$  and its adjoint  $\widetilde{\mathcal{DIV}} \cong -\mathcal{GRAD}^*$  implies that

$$\langle q^N, \widetilde{\mathcal{DIV}} \mathbf{w}^{\mathcal{E}} \rangle_N = -\langle q^N, \mathcal{GRAD}^* \mathbf{w}^{\mathcal{E}} \rangle_N = -\langle \mathcal{GRAD} q^N, \mathbf{w}^{\mathcal{E}} \rangle_{\mathcal{E}} \quad \forall q^N \in N, \mathbf{w}^{\mathcal{E}} \in \mathcal{E} \tag{25}$$

from which we obtain that

$$\widetilde{\mathcal{DIV}} = -\mathbb{M}^{N-1} \mathcal{GRAD}^T \mathbb{M}^{\mathcal{E}}. \tag{26}$$

## 4. Definition of $P_0$ -consistent reconstruction operators

In this section we define the novel concept of  $P_0$ -consistent reconstruction operators and provide its geometric counterpart. The definition relies on a commuting diagram property of the discrete dual de Rham complex which involves the derived discrete operators and characterizes in a rigorous way the class of all reconstruction operators that can be used to construct a global mass matrix in a such a way that a global patch test is passed. Thus, the  $P_0$ -consistency of reconstruction operators refers to the property that we able to reproduce exactly the continuous solution at the discrete level. Instead, the consistency condition (14) only expresses an equivalence between discrete and continuous energy, and thus, it is a necessary but not sufficient condition. The geometry enters into the scheme since for low-order numerical schemes only averages of reconstruction operators over a given region are measured. In such a case, the matrix representation of the average reconstruction operator has entries which can be interpreted as familiar geometric elements of the space, like segments and polygons. The geometric conditions that characterize the class of  $P_0$ -consistent reconstruction operators can be written as a linear system of equations. A closer inspection of this linear system reveals that in general it does not have a unique solution. Thus, there is no unique way of designing  $P_0$ -consistent reconstruction operators.

#### 4.1. $P_0$ -consistent face reconstruction operators

Let us consider the example of magnetic phenomena as described by the following equations

$$\begin{aligned}\nabla \times \mathbf{H} &= \mathbf{J}, \\ \nabla \cdot \mathbf{B} &= 0, \\ \mathbf{H} &= \mathbf{v}\mathbf{B}, \\ \mathbf{H} \times \mathbf{n} &= \mathbf{J}_s,\end{aligned}\tag{27}$$

where the source of the problem is a known current density vector field  $\mathbf{J}$ . In particular, let us consider boundary conditions in such a way that vector fields  $\mathbf{B}$ ,  $\mathbf{H}$  are constant in  $\Omega$ . In this situation, Ampère's law must be  $\nabla \times \mathbf{H} = \mathbf{J} = \mathbf{0}$ .

To introduce the corresponding mimetic form of the above equations, let  $\mathbf{B}^{\mathcal{F}}$  be the DoFs of the vector field  $\mathbf{B}$  attached to faces of the grid. We represent the divergence and curl operators that appear in (27) by the discrete operator  $\mathcal{DIV}$  and the derived operator  $\widetilde{\mathcal{CURL}}$ . Using these operators, the mimetic discretization of (27) reads as follows

$$\mathcal{DIV} \mathbf{B}^{\mathcal{F}} = \mathbf{0},\tag{28}$$

$$\widetilde{\mathcal{CURL}} \mathbf{B}^{\mathcal{F}} = \mathbf{0}.\tag{29}$$

Due to the Dirichlet boundary conditions, (29) should be considered only for the interior edges. By using (24), (29) can be equivalently written as follows

$$\mathbb{M}^{\mathcal{E}-1} \mathcal{CURL}^T \mathbb{M}^{\mathcal{F}} \mathbf{B}^{\mathcal{F}} = \mathbf{0}.\tag{30}$$

We left multiply (30) by  $\mathbb{M}^{\mathcal{E}}$  obtaining

$$\mathcal{CURL}^T \left( \sum_{c \in \mathcal{C}} (\mathbb{S}_c^{\mathcal{F}})^T |c| (\mathbb{R}_c^{\mathcal{F}})^T \mathbf{v} \mathbb{R}_c^{\mathcal{F}} \mathbb{S}_c^{\mathcal{F}} \right) \mathbf{B}^{\mathcal{F}} = \mathbf{0},\tag{31}$$

where we have used (20) for the definition of the global mass matrix  $\mathbb{M}^{\mathcal{F}}$ . Next, by using  $\mathbf{H} = \mathbf{v}\mathbf{B}$ , it follows that

$$\mathcal{CURL}^T \left( \sum_{c \in \mathcal{C}} (\mathbb{S}_c^{\mathcal{F}})^T |c| (\mathbb{R}_c^{\mathcal{F}})^T \right) \mathbf{H} = \mathbf{0}.\tag{32}$$

Finally, since  $\mathbf{H} \in \mathbb{R}^3$  is arbitrary, we obtain the following *geometric condition*

$$\text{row}_e \mathbb{C}^T \left( \sum_{c \in \mathcal{C}} (\mathbb{S}_c^{\mathcal{F}})^T |c| (\mathbb{R}_c^{\mathcal{F}})^T \right) = \mathbf{0}, \quad \forall e \in E, e \not\subset \partial\Omega\tag{33}$$

where we have used the matrix form of the  $\mathcal{CURL}$  operator.

A dimensional analysis informs us that each entry of matrix  $|c| (\mathbb{R}_c^{\mathcal{F}})^T$  has units of linear meters. This is a direct consequence of the property of  $\mathbb{R}_c^{\mathcal{F}}$  of being a left inverse of  $\mathbb{P}_c^{\mathcal{F}}$ . Given the physical dimensions, rows of  $|c| (\mathbb{R}_c^{\mathcal{F}})^T$  can be regarded as geometric *edges* and (33) requires that they can be put one after the other to form a geometric closed path. Thus, they encode the geometric structure of a set of edges of a grid.

**Definition 4.1** ( $P_0$ -consistent face reconstruction operators). A collection of reconstruction operators  $\{\mathbb{R}_c^{\mathcal{F}}\}_{c \in \mathcal{C}}$  is said to be  $P_0$ -consistent if and only if the following *geometric condition* holds

$$\text{row}_e \mathbb{C}^T \left( \sum_{c \in \mathcal{C}} (\mathbb{S}_c^{\mathcal{F}})^T |c| (\mathbb{R}_c^{\mathcal{F}})^T \right) = \mathbf{0}, \quad \forall e \in E, e \not\subset \partial\Omega.\tag{34}$$

#### 4.2. $P_0$ -consistent edge reconstruction operators

Let us consider the example of electric phenomena as described by the following equations

$$\begin{aligned}\nabla \times \mathbf{E} &= \mathbf{0}, \\ \nabla \cdot \mathbf{D} &= \rho, \\ \mathbf{D} &= \epsilon \mathbf{E}, \\ \mathbf{D} \cdot \mathbf{n} &= \rho_s,\end{aligned}\tag{35}$$

where the source of the problem is a known charge density scalar field  $\rho$ . In particular, let us consider boundary conditions in such a way that vector fields  $\mathbf{E}$ ,  $\mathbf{D}$  are constant in  $\Omega$ . In this situation, Gauss' law must be  $\nabla \cdot \mathbf{D} = 0$ .

To introduce the corresponding mimetic form of the above equations, let  $\mathbf{E}^\mathcal{E}$  be the DoFs of the vector field  $\mathbf{E}$  attached to edges of the grid. We represent the curl and divergence operators that appear in (35) by the discrete operator  $\mathcal{CURL}$  and the derived operator  $\widetilde{\mathcal{DIV}}$ . Using these operators, the mimetic discretization of (35) reads as follows

$$\mathcal{CURL} \mathbf{E}^\mathcal{E} = \mathbf{0}, \quad (36)$$

$$\widetilde{\mathcal{DIV}} \mathbf{E}^\mathcal{E} = \mathbf{0}. \quad (37)$$

Due to the Dirichlet boundary conditions, (37) should be considered only for the interior nodes. By using (26), (37) can be equivalently written as follows

$$-\mathbb{M}^{N-1} \mathcal{GRAD}^T \mathbb{M}^\mathcal{E} \mathbf{E}^\mathcal{E} = \mathbf{0}. \quad (38)$$

We left multiply (38) by  $\mathbb{M}^N$  obtaining

$$\mathcal{DIV}^T \left( \sum_{c \in \mathcal{C}} (\mathbb{S}_c^\mathcal{E})^T |c| (\mathbb{R}_c^\mathcal{E})^T \mathbf{v} \mathbb{R}_c^\mathcal{E} \mathbb{S}_c^\mathcal{E} \right) \mathbf{E}^\mathcal{E} = \mathbf{0}, \quad (39)$$

where we have used (20) for the definition of the global mass matrix  $\mathbb{M}^\mathcal{E}$ . Next, by using  $\mathbf{D} = \boldsymbol{\epsilon} \mathbf{E}$ , it follows that

$$\mathcal{DIV}^T \left( \sum_{c \in \mathcal{C}} (\mathbb{S}_c^\mathcal{E})^T |c| (\mathbb{R}_c^\mathcal{E})^T \right) \mathbf{D} = \mathbf{0}. \quad (40)$$

Finally, since  $\mathbf{D} \in \mathbb{R}^3$  is arbitrary, we obtain the following *geometric condition*

$$\text{row}_n \mathbb{G}^T \left( \sum_{c \in \mathcal{C}} (\mathbb{S}_c^\mathcal{E})^T |c| (\mathbb{R}_c^\mathcal{E})^T \right) = \mathbf{0}, \quad \forall n \in N, n \notin \partial \Omega \quad (41)$$

where we have used the matrix form of the  $\mathcal{DIV}$  operator.

A dimensional analysis informs us that each entry of matrix  $|c| (\mathbb{R}_c^\mathcal{E})^T$  has units of square meters. This is a direct consequence of the property of  $\mathbb{R}_c^\mathcal{E}$  of being a left inverse of  $\mathbb{P}_c^\mathcal{E}$ . Given the physical dimensions, rows of  $|c| (\mathbb{R}_c^\mathcal{E})^T$  can be regarded as *geometric faces* and (41) requires that they can be put side to side to form a geometric closed surface. Thus, they encode the geometric structure of a set of faces of a grid.

**Definition 4.2** ( *$P_0$ -consistent edge reconstruction operators*). A collection of reconstruction operators  $\{\mathbb{R}_c^\mathcal{E}\}_{c \in \mathcal{C}}$  is said to be  $P_0$ -consistent if and only if the following *geometric condition* holds

$$\text{row}_n \mathbb{G}^T \left( \sum_{c \in \mathcal{C}} (\mathbb{S}_c^\mathcal{E})^T |c| (\mathbb{R}_c^\mathcal{E})^T \right) = \mathbf{0}, \quad \forall n \in N, n \notin \partial \Omega. \quad (42)$$

#### 4.3. Linear system formulation of $P_0$ -consistent reconstruction operators

The two requirements that reconstruction operators have to satisfy can be encoded into a linear system of equations. The unknown variables are the entries of the matrices  $|c| (\mathbb{R}_c^\mathcal{E})^T$ ,  $|c| (\mathbb{R}_c^\mathcal{F})^T$  with constraint equations expressed by (34), (42) and the requirement that each matrix  $\mathbb{R}_c^\mathcal{E}$  and  $\mathbb{R}_c^\mathcal{F}$  is a left inverse of the local projection operator, which is the accuracy property for constant vector fields. More specifically, we can write

$$\begin{cases} \mathbb{R}_c^\mathcal{F} \mathbb{P}_c^\mathcal{F} = \mathbb{I}_3, \quad \forall c \in \mathcal{C} \\ \text{row}_e \mathbb{C}^T \left( \sum_{c \in \mathcal{C}} (\mathbb{S}_c^\mathcal{F})^T |c| (\mathbb{R}_c^\mathcal{F})^T \right) = \mathbf{0}, \quad \forall e \in E, e \notin \partial \Omega \end{cases} \quad (43)$$

and

$$\begin{cases} \mathbb{R}_c^\mathcal{E} \mathbb{P}_c^\mathcal{E} = \mathbb{I}_3, \quad \forall c \in \mathcal{C} \\ \text{row}_n \mathbb{G}^T \left( \sum_{c \in \mathcal{C}} (\mathbb{S}_c^\mathcal{E})^T |c| (\mathbb{R}_c^\mathcal{E})^T \right) = \mathbf{0}, \quad \forall n \in N, n \notin \partial \Omega \end{cases} \quad (44)$$

where  $\mathbb{I}_3$  denotes the identity matrix of dimension 3.

A canonical solution of the two systems of equations is given by the barycentric dual grid. While the geometric conditions in (34) and (42) are trivially satisfied, proofs that geometric elements of the dual grid satisfy also the accuracy property are given in the next section. Other solutions are known for particular cell shapes. For instance, for cubical cells [1] and Delaunay tetrahedral grids [16], Voronoi dual grids are well defined and satisfy the above properties. In general, the above linear systems do not have a unique solution, see Example 1.

The design of other  $P_0$ -consistent reconstruction operators is a global process since it links reconstruction operators defined on more than one cell. A crucial observation is the following: if we design reconstruction operator at the single element level, without taking into account adjacent cells, the dual barycentric grid is the unique canonical choice to design reconstruction operators for arbitrary polyhedral elements.

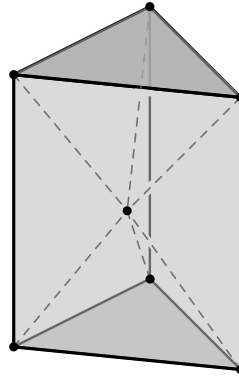


Fig. 2. Polyhedral grid made by 2 tetrahedra and 3 square pyramids.

**Example 1** (*Geometric conditions for a polyhedral grid*). Let us consider the polyhedral grid  $K$  pictured in Fig. 2. The grid is made by 5 cells and 14 faces. As an instance, we analyze the dimension of the affine solution space of the linear system (44). We satisfy the constraint expressed by the geometric conditions by identifying with the same unknown the unique two unknowns vector variables corresponding to the same face which lies at the intersection of two cells. Thus, we have 14 unknowns vectors variables each associated with a face of  $K$ . The requirement that the matrix  $\mathbb{R}_c^{\mathcal{F}}$  is a left inverse of  $\mathbb{F}_c$  for every cell  $c$  of  $K$  is encoded into a constraint matrix of size  $15 \times 14$ . A direct computation reveals that the rank of this constraint matrix is 12. Since there exists at least a solution, which is given by the coordinates of the barycenters of faces of  $K$ , see Section 5, the system is consistent, and we have an infinite number of solutions since the constraint matrix is rank deficient.

As a consequence of the conditions (34), (42), the geometric entries of the reconstruction operators on every element are defined up to an arbitrary point in  $\mathbb{R}^3$ . This latter can be chosen freely and can be used to optimize reconstruction operators. We explore this possibility in the next section.

## 5. Dual grid $P_0$ -consistent reconstruction operators

In this section we prove that reconstruction operators defined in [23] are equivalent to reconstruction operators defined by geometric elements of the barycentric dual grid. The main novelty with respect to the proofs given in [23] relies on the explicit identification of geometrical elements of dual faces in the expression of edge reconstruction operators. Since geometric elements of the barycentric dual grid satisfy the geometric conditions (34) and (42), the analysis reveals the role of the barycentric dual grid in low-order compatible numerical schemes: even if the dual grid is not assumed as a starting point of the method, for instance in mimetic literature [8], it appears as a canonical choice of constructing  $P_0$ -consistent reconstruction operators. According to the results derived in Section 4, the expressions of the reconstruction formulas inform us that they are defined up to an arbitrary point in  $\mathbb{R}^3$ . We show how this freedom of choice in the design of reconstruction formulas can be used to optimize specific objective functions.

### 5.1. Reconstruction formulas and their proofs

Let us consider a pair of vector fields  $\mathbf{u}, \mathbf{w} : \mathbb{R}^3 \rightarrow \mathbb{R}^3$  along with a scalar field  $w : \mathbb{R}^3 \rightarrow \mathbb{R}$  defined on a given cell  $c$ . The following well-known integration by parts formulas hold

$$\int_c \mathbf{u} \cdot \nabla w dV = - \int_c \nabla \cdot \mathbf{u} w dV + \int_{\partial c} \mathbf{u} \cdot \mathbf{n} w dS, \quad (45)$$

$$\int_c \mathbf{u} \cdot \nabla \times \mathbf{w} dV = \int_c \nabla \times \mathbf{u} \cdot \mathbf{w} dV + \int_{\partial c} \mathbf{u} \times \mathbf{n} \cdot \mathbf{w} dS. \quad (46)$$

Given a cell  $c$ , we write “ $f \in \partial c$ ” meaning that  $f$  is varying over all (oriented) faces of  $c$ . Similarly, we write “ $e \in \partial c$ ” meaning that  $e$  is varying over all (oriented) edges of  $c$ . Finally, given a polygon  $f$  in some (affine) plane of  $\mathbb{R}^3$ , we write “ $e \in \partial f$ ” meaning that  $e$  is varying over all (suitably oriented) edges of the boundary of  $f$ .

**Theorem 2** (*Reconstruction from face DoFs*). Let  $\mathbf{u}$  be a constant vector field defined on a cell  $c$ . Choose an arbitrary dual node  $\tilde{\mathbf{n}}_c \in \mathbb{R}^3$  and define  $\tilde{\mathbf{e}}_f := \mathbf{b}_f - \tilde{\mathbf{n}}_c$ , as at the end of Section 2. The following equality holds

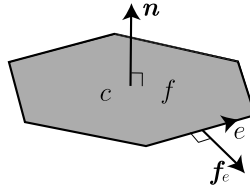


Fig. 3. A polygon and the relevant geometric elements involved in the proof of Lemma 2.

$$\mathbf{u} = \frac{1}{|c|} \sum_{f \in \partial c} (\mathbf{u} \cdot \mathbf{f}) \tilde{\mathbf{e}}_f. \tag{47}$$

**Proof.** Let  $\mathbf{w} \in \mathbb{R}^3$ . Thanks to (45), we have

$$|c| \mathbf{u} \cdot \mathbf{w} = \int_c \mathbf{u} \cdot \mathbf{w} dV = \int_c \mathbf{u} \cdot \nabla (\mathbf{w} \cdot (\mathbf{x} - \tilde{\mathbf{n}}_c)) dV = \int_{\partial c} (\mathbf{u} \cdot \mathbf{n}) (\mathbf{w} \cdot (\mathbf{x} - \tilde{\mathbf{n}}_c)) dS = \sum_{f \in \partial c} (\mathbf{u} \cdot \mathbf{f}) ((\mathbf{b}_f - \tilde{\mathbf{n}}_c) \cdot \mathbf{w}). \tag{48}$$

By using the definition of  $\tilde{\mathbf{e}}_f$ , it follows that

$$|c| \mathbf{u} \cdot \mathbf{w} = \sum_{f \in \partial c} (\mathbf{u} \cdot \mathbf{f}) (\tilde{\mathbf{e}}_f \cdot \mathbf{w}). \tag{49}$$

Since  $\mathbf{w}$  is arbitrary, we obtain the claimed equality.  $\square$

**Lemma 2** (Reconstruction from edge DoFs restricted to a polygonal face). Let  $\mathbf{u}$  be a constant vector field and let  $f$  be a polygon in some plane  $L$  of  $\mathbb{R}^3$ . Let us denote with  $\mathbf{n}$  the unit vector orthogonal to  $f$ . Choose an arbitrary point  $\mathbf{p} \in \mathbb{R}^3$ . The following equality holds

$$\mathbf{u} \times \mathbf{n} = \frac{1}{|f|} \sum_{e \in \partial f} (\mathbf{u} \cdot \mathbf{e}) (\mathbf{b}_e - \mathbf{p}). \tag{50}$$

**Proof.** Let  $\mathbf{f}_e := \mathbf{e} \times \mathbf{n}$  be the vector orthogonal to edge  $e$  in  $L$ . Note that vector  $\mathbf{u} \times \mathbf{n}$  belongs to  $L$ . Thus, if we apply the argument used in the proof of Theorem 2 to the vector field  $\mathbf{u} \times \mathbf{n}$  restricted to  $f$ , then we obtain

$$\mathbf{u} \times \mathbf{n} = \frac{1}{|f|} \sum_{e \in \partial f} ((\mathbf{u} \times \mathbf{n}) \cdot \mathbf{f}_e) (\mathbf{b}_e - \mathbf{p}). \tag{51}$$

Based on the definition of  $\mathbf{f}_e$ , it follows that

$$(\mathbf{u} \times \mathbf{n}) \cdot \mathbf{f}_e = (\mathbf{u} \times \mathbf{n}) \cdot (\mathbf{e} \times \mathbf{n}) = (\mathbf{n} \times (\mathbf{u} \times \mathbf{n})) \cdot \mathbf{e} = \mathbf{u} \cdot \mathbf{e}. \tag{52}$$

and hence, substituting in (51), we obtain the claimed equality (see Fig. 3).  $\square$

**Theorem 3** (Reconstruction from edge DoFs). Let  $\mathbf{u}$  be a constant vector field defined on a cell  $c$ . Choose an arbitrary dual node  $\tilde{\mathbf{n}}_c \in \mathbb{R}^3$  and define  $\tilde{\mathbf{f}}_e$  as at the end of Section 2. The following equality holds

$$\mathbf{u} = \frac{1}{|c|} \sum_{e \in \partial c} (\mathbf{u} \cdot \mathbf{e}) \tilde{\mathbf{f}}_e. \tag{53}$$

**Proof.** Let  $\mathbf{w} \in \mathbb{R}^3$ . Thanks to (46), we have

$$\begin{aligned} 2|c| \mathbf{u} \cdot \mathbf{w} &= 2 \int_c \mathbf{u} \cdot \mathbf{w} dV = \int_c \mathbf{u} \cdot \nabla \times (\mathbf{w} \times (\mathbf{x} - \tilde{\mathbf{n}}_c)) dV = \int_{\partial c} (\mathbf{u} \times \mathbf{n}) \cdot (\mathbf{w} \times (\mathbf{x} - \tilde{\mathbf{n}}_c)) dS \\ &= \sum_{f \in \partial c} \int_f (\mathbf{u} \times \mathbf{n}_f) \cdot (\mathbf{w} \times (\mathbf{x} - \tilde{\mathbf{n}}_c)) dS = \sum_{f \in \partial c} |f| (\mathbf{u} \times \mathbf{n}_f) \cdot (\mathbf{w} \times \tilde{\mathbf{e}}_f). \end{aligned} \tag{54}$$

Apply Lemma 2 to every face  $f$  in the last term of the above expression, choosing the same node  $\tilde{\mathbf{n}}_c$  as the arbitrary point involved in the formula. We obtain

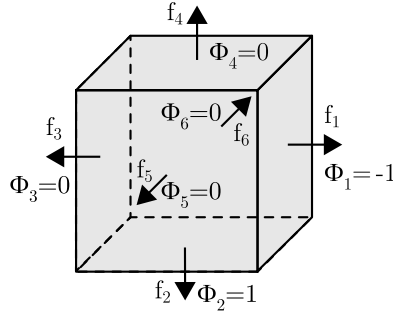


**Fig. 4.** A cubic cell  $c$ . A set of DoFs  $\Phi$  are attached to faces. This is an example of DoFs that are not image of any constant vector field under the projection map  $\mathbb{P}_c^{\mathcal{F}}$ .

$$\begin{aligned}
 2|c|\mathbf{u} \cdot \mathbf{w} &= \sum_{f \in \partial c} \left( \sum_{e \in \partial f} (\mathbf{u} \cdot \mathbf{e})(\mathbf{b}_e - \tilde{\mathbf{n}}_c) \right) \cdot (\mathbf{w} \times \tilde{\mathbf{e}}_f) = \sum_{f \in \partial c} \left( \tilde{\mathbf{e}}_f \times \left( \sum_{e \in \partial f} (\mathbf{u} \cdot \mathbf{e})(\mathbf{b}_e - \tilde{\mathbf{n}}_c) \right) \right) \cdot \mathbf{w} \\
 &= \sum_{e \in \partial c} (\mathbf{u} \cdot \mathbf{e}) \left( (\tilde{\mathbf{e}}_{f_i} \times (\mathbf{b}_e - \tilde{\mathbf{n}}_c) - \tilde{\mathbf{e}}_{f_j} \times (\mathbf{b}_e - \tilde{\mathbf{n}}_c)) \cdot \mathbf{w} \right),
 \end{aligned} \tag{55}$$

where  $f_i, f_j$  are the unique faces of  $c$  such that  $e = f_i \cap f_j$ , for suitable indices  $i = i(e)$  and  $j = j(e)$ , and oriented so that they induce opposite orientations on edge  $e$ . Now, dividing by two both members of the last term in (55) and using the definition of  $\tilde{\mathbf{f}}_e$ , it follows that

$$|c|\mathbf{u} \cdot \mathbf{w} = \sum_{e \in \partial c} (\mathbf{u} \cdot \mathbf{e})(\tilde{\mathbf{f}}_e \cdot \mathbf{w}). \tag{56}$$

Since  $\mathbf{w}$  is arbitrary, we obtain the claimed equality.  $\square$

**Lemma 3** (Dual grid reconstruction operators). *Let us consider a cell  $c$ . Choose an arbitrary dual node  $\tilde{\mathbf{n}}_c \in \mathbb{R}^3$ . Let  $\mathbb{R}_{\tilde{\mathbf{n}}_c}^{\mathcal{F}} := \frac{1}{|c|} (\mathbb{P}_{\tilde{\mathbf{n}}_c}^{\tilde{\mathcal{E}}})^T$  and  $\mathbb{R}_{\tilde{\mathbf{n}}_c}^{\mathcal{E}} := \frac{1}{|c|} (\mathbb{P}_{\tilde{\mathbf{n}}_c}^{\tilde{\mathcal{F}}})^T$ . The following formulas hold*

$$\mathbb{R}_{\tilde{\mathbf{n}}_c}^{\mathcal{F}} \mathbb{P}_c^{\mathcal{F}} = \mathbb{I}_3, \tag{57}$$

$$\mathbb{R}_{\tilde{\mathbf{n}}_c}^{\mathcal{E}} \mathbb{P}_c^{\mathcal{E}} = \mathbb{I}_3. \tag{58}$$

**Proof.** By using Theorem 2, Theorem 3 and the definition of the matrices  $\mathbb{P}_{\tilde{\mathbf{n}}_c}^{\tilde{\mathcal{E}}}, \mathbb{P}_{\tilde{\mathbf{n}}_c}^{\tilde{\mathcal{F}}}$ , we have the following identities  $(\mathbb{P}_{\tilde{\mathbf{n}}_c}^{\tilde{\mathcal{E}}})^T \mathbb{P}_c^{\mathcal{F}} = |c| \mathbb{I}_3, (\mathbb{P}_{\tilde{\mathbf{n}}_c}^{\tilde{\mathcal{F}}})^T \mathbb{P}_c^{\mathcal{E}} = |c| \mathbb{I}_3$ . Dividing by  $|c|$  both members of the latter equations we obtain the claimed result.  $\square$

### 5.2. Optimizing dual grid reconstruction operators

The expressions of the dual grid reconstruction operators show that they are uniquely defined up to an arbitrary point  $\tilde{\mathbf{n}}_c \in \mathbb{R}^3$ , which can be chosen independently for every cell. Now, we show how this fact can be used to optimize the dual grid reconstruction operators. In particular, we ask if for a given cell  $c$  there exists a point such that the reconstructed vector field is optimal with respect to a least square difference.

Let  $\mathcal{X} = \mathcal{E}$  or  $\mathcal{X} = \mathcal{F}$ . We observe that the map  $\mathbb{P}_c^{\mathcal{X}}$  has rank 3, thus it is not surjective as a map from  $\mathbb{R}^3$  to  $\mathbb{R}^{\dim(\mathcal{X}_c)}$ , see Fig. 4.

Let  $\mathbf{u}_c^{\mathcal{X}} \notin \text{im } \mathbb{P}_c^{\mathcal{X}}$ . In this case, among all possible constant vector fields, we select the minimum norm solution of the following least squares problem

$$\mathbf{u}^* = \arg \min_{\mathbf{u} \in \mathbb{R}^3} \left\| \mathbb{P}_c^{\mathcal{X}} \mathbf{u} - \mathbf{u}_c^{\mathcal{X}} \right\|_2. \tag{59}$$

The Moore–Penrose matrix inverse of  $\mathbb{P}_c^{\mathcal{X}}$ , denoted as  $(\mathbb{P}_c^{\mathcal{X}})^+$ , allows us to write the minimum norm solution  $\mathbf{u}^*$  of (59) into the following form

$$\mathbf{u}^* = (\mathbb{P}_c^{\mathcal{X}})^+ \mathbf{u}_c^{\mathcal{X}}; \tag{60}$$

moreover, since  $\mathbb{X}_c$  has full rank,  $(\mathbb{P}_c^{\mathcal{X}})^+$  can be explicitly written as  $(\mathbb{P}_c^{\mathcal{X}})^+ = (\mathbb{P}_c^{\mathcal{X}})^T \mathbb{P}_c^{\mathcal{X}})^{-1} (\mathbb{P}_c^{\mathcal{X}})^T$ , see [26].

Now, we ask the following question: does there exist a point  $\tilde{\mathbf{n}}_c \in \mathbb{R}^3$  such that  $\mathbb{R}_{\tilde{\mathbf{n}}_c}^{\mathcal{X}} = (\mathbb{P}_c^{\mathcal{X}})^+$ ? By Lemma 3, we know that  $\mathbb{R}_{\tilde{\mathbf{n}}_c}^{\mathcal{X}}$  is a left inverse of  $\mathbb{P}_c^{\mathcal{X}}$ . Thus, in order that  $\mathbb{R}_{\tilde{\mathbf{n}}_c}^{\mathcal{X}} = (\mathbb{P}_c^{\mathcal{X}})^+$ , it is sufficient that the following property holds

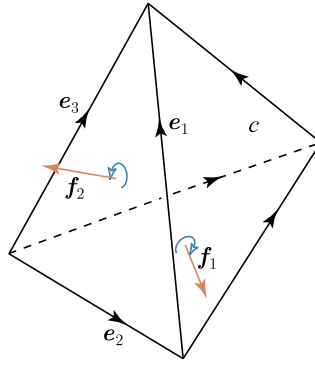


Fig. 5. A tetrahedron to illustrate the geometric quantities involved in the proof of Lemma 4.

$$\mathbb{P}_c^{\mathcal{X}} \mathbb{R}_{\tilde{\mathbf{n}}_c}^{\mathcal{X}} = (\mathbb{P}_c^{\mathcal{X}} \mathbb{R}_{\tilde{\mathbf{n}}_c}^{\mathcal{X}})^T, \tag{61}$$

see [26]. For tetrahedral and cubic cells we have the following characterization.

**Lemma 4.** Let  $c$  be a tetrahedral or cubic cell. If  $\tilde{\mathbf{n}}_c$  is the barycenter of  $c$ , then  $\tilde{\mathbf{n}}_c$  satisfies (61).

**Proof.** First, suppose that  $c$  is a tetrahedron, see the tetrahedron pictured in Fig. 5. Consider the case  $\mathcal{X} = \mathcal{F}$ . We have to show that  $\mathbb{P}_c^{\mathcal{F}} \mathbb{R}_{\tilde{\mathbf{n}}_c}^{\mathcal{F}}$  is symmetric. It is sufficient to consider the pair of faces  $\mathbf{f}_1$  and  $\mathbf{f}_2$ . By definition, we have

$$\mathbf{f}_1 \cdot \tilde{\mathbf{e}}_2 = \left( \frac{\mathbf{e}_1 \times \mathbf{e}_2}{2} \right) \cdot \left( \frac{\mathbf{e}_2 + \mathbf{e}_3}{3} - \frac{\mathbf{e}_1 + \mathbf{e}_2 + \mathbf{e}_3}{4} \right) = \frac{1}{24} (\mathbf{e}_1 \times \mathbf{e}_2) \cdot \mathbf{e}_3, \tag{62}$$

$$\mathbf{f}_2 \cdot \tilde{\mathbf{e}}_1 = \left( \frac{\mathbf{e}_2 \times \mathbf{e}_3}{2} \right) \cdot \left( \frac{\mathbf{e}_1 + \mathbf{e}_2}{3} - \frac{\mathbf{e}_1 + \mathbf{e}_2 + \mathbf{e}_3}{4} \right) = \frac{1}{24} (\mathbf{e}_2 \times \mathbf{e}_3) \cdot \mathbf{e}_1. \tag{63}$$

By comparing the above two expressions we obtain  $\mathbf{f}_1 \cdot \tilde{\mathbf{e}}_2 = \mathbf{f}_2 \cdot \tilde{\mathbf{e}}_1$ .

Consider now the case  $\mathcal{X} = \mathcal{E}$ . Let us prove that  $\mathbb{P}_c^{\mathcal{E}} \mathbb{R}_{\tilde{\mathbf{n}}_c}^{\mathcal{E}}$  is symmetric. It is sufficient to consider the pair of edges  $\mathbf{e}_1$  and  $\mathbf{e}_2$ . By definition, we have

$$\tilde{\mathbf{f}}_1 \cdot \mathbf{e}_2 = \left( \frac{1}{2} \left( \frac{\mathbf{e}_1 + \mathbf{e}_2}{3} - \frac{\mathbf{e}_1 + \mathbf{e}_3}{3} \right) \times \left( \frac{\mathbf{e}_1}{2} - \frac{\mathbf{e}_1 + \mathbf{e}_2 + \mathbf{e}_3}{4} \right) \right) \cdot \mathbf{e}_2 = \frac{1}{24} (\mathbf{e}_1 \times \mathbf{e}_3) \cdot \mathbf{e}_2, \tag{64}$$

$$\tilde{\mathbf{f}}_2 \cdot \mathbf{e}_1 = \left( \frac{1}{2} \left( \frac{\mathbf{e}_2 + \mathbf{e}_3}{3} - \frac{\mathbf{e}_1 + \mathbf{e}_2}{3} \right) \times \left( \frac{\mathbf{e}_2}{2} - \frac{\mathbf{e}_1 + \mathbf{e}_2 + \mathbf{e}_3}{4} \right) \right) \cdot \mathbf{e}_1 = \frac{1}{24} (\mathbf{e}_3 \times \mathbf{e}_2) \cdot \mathbf{e}_1. \tag{65}$$

By comparing the above two expressions we obtain  $\tilde{\mathbf{f}}_1 \cdot \mathbf{e}_2 = \tilde{\mathbf{f}}_2 \cdot \mathbf{e}_1$ .

Let  $c$  be a cubic cell. Consider the case  $\mathcal{X} = \mathcal{F}$ . We have to show that  $\mathbb{P}_c^{\mathcal{F}} \mathbb{R}_{\tilde{\mathbf{n}}_c}^{\mathcal{F}}$  is symmetric. Observe that the  $(i, j)$ -entry of this product is of the form  $\mathbf{f}_i \cdot \tilde{\mathbf{e}}_{f_j}$  for some pair of faces  $\mathbf{f}_i, \mathbf{f}_j$ . Let  $i \neq j$ . Define  $\tilde{\mathbf{e}}_i := \tilde{\mathbf{e}}_{f_i}$  and  $\tilde{\mathbf{e}}_j := \tilde{\mathbf{e}}_{f_j}$ . Two cases are possible, either  $\mathbf{f}_i = -\mathbf{f}_j$  or  $\mathbf{f}_i \cdot \mathbf{f}_j = 0$ . In the first case, we have  $\tilde{\mathbf{e}}_i = -\tilde{\mathbf{e}}_j$  from which follows that  $\mathbf{f}_i \cdot \tilde{\mathbf{e}}_j = \mathbf{f}_j \cdot \tilde{\mathbf{e}}_i$ . In the second case, we have  $\mathbf{f}_i \cdot \tilde{\mathbf{e}}_j = 0$  and  $\mathbf{f}_j \cdot \tilde{\mathbf{e}}_i = 0$ , from which follows that  $\mathbf{f}_i \cdot \tilde{\mathbf{e}}_j = \mathbf{f}_j \cdot \tilde{\mathbf{e}}_i$ .

Consider now the case  $\mathcal{X} = \mathcal{E}$ . Let us prove that  $\mathbb{P}_c^{\mathcal{E}} \mathbb{R}_{\tilde{\mathbf{n}}_c}^{\mathcal{E}}$  is symmetric. Observe that the  $(i, j)$ -entry of this product is of the form  $\mathbf{e}_i \cdot \tilde{\mathbf{f}}_{e_j}$  for some pair of edges  $\mathbf{e}_i, \mathbf{e}_j$ . Let  $i \neq j$ . Define  $\tilde{\mathbf{f}}_i := \tilde{\mathbf{f}}_{e_i}$  and  $\tilde{\mathbf{f}}_j := \tilde{\mathbf{f}}_{e_j}$ . Two cases are possible, either  $\mathbf{e}_i = \pm \mathbf{e}_j$  or  $\mathbf{e}_i \cdot \mathbf{e}_j = 0$ . In the first case, we have  $\tilde{\mathbf{f}}_i = \pm \tilde{\mathbf{f}}_j$  from which follows that  $\mathbf{e}_i \cdot \tilde{\mathbf{f}}_j = \mathbf{e}_j \cdot \tilde{\mathbf{f}}_i$ . In the second case, we have  $\mathbf{e}_i \cdot \tilde{\mathbf{f}}_j = 0$  and  $\mathbf{e}_j \cdot \tilde{\mathbf{f}}_i = 0$  from which follows that  $\mathbf{e}_i \cdot \tilde{\mathbf{f}}_j = \mathbf{e}_j \cdot \tilde{\mathbf{f}}_i$ .  $\square$

Let us denote by  $D$  the set of all cells that satisfy (61) for some point  $\tilde{\mathbf{n}}_c \in \mathbb{R}^3$ .

**Example 4.** Let us consider the case of the face reconstruction operator  $\mathbb{R}_{\tilde{\mathbf{n}}_c}^{\mathcal{F}}$ . By definition, we have  $\mathbb{R}_{\tilde{\mathbf{n}}_c}^{\mathcal{F}} = \frac{1}{|c|} (\mathbb{P}_c^{\mathcal{E}} - \mathbf{1} \tilde{\mathbf{n}}_c^T)^T$ , where  $\mathbf{1}$  denotes the vector in  $\mathbb{R}^{\text{card}(F_c)}$  whose entries are all equal to 1. Let us consider a pyramid with a square base divided in two triangles. The boundary decomposes into six faces. A direct computation reveals that this cell does not belong to  $D$ . To show this, it is sufficient to directly compute the Moore–Penrose matrix inverse  $(\mathbb{P}_c^{\mathcal{F}})^+$  and subtract from  $(\mathbb{P}_c^{\mathcal{E}})^T$  the matrix  $|c|(\mathbb{P}_c^{\mathcal{F}})^+$ . If there exists a point  $\tilde{\mathbf{n}}_c$  satisfying (61), then the columns of this matrix difference must be all equal to  $\tilde{\mathbf{n}}_c$ .

To handle the situations where a cell  $c \notin D$ , we propose to select a dual node  $\tilde{\mathbf{n}}_c$  which minimizes the distance with respect to the Moore–Penrose inverse matrix measured by a  $L^2$  metric.

**Definition 5.1** (Optimal dual node). Let us introduce the following map

$$\begin{aligned} \xi_c: \mathbb{R}^3 &\rightarrow \mathbb{R} \\ \tilde{\mathbf{n}}_c &\mapsto \left\| \mathbb{R}_{\tilde{\mathbf{n}}_c}^{\mathcal{X}} - (\mathbb{P}_c^{\mathcal{X}})^+ \right\|_2^2. \end{aligned} \quad (66)$$

We define the *optimal dual node* of a cell  $c$ ,  $\tilde{\mathbf{n}}_{\text{opt},c}$ , as the unique point which minimizes function  $\xi_c$ .

From the practical point of view we can solve the optimization problem in (66) for every cell and find two optimal reference points, one for the matrix  $\mathbb{R}_{\tilde{\mathbf{n}}_c}^{\mathcal{F}}$  and the other one for  $\mathbb{R}_{\tilde{\mathbf{n}}_c}^{\mathcal{E}}$ . To speed up the computation we choose a unique point as the optimal dual node of the matrix  $\mathbb{R}_{\tilde{\mathbf{n}}_c}^{\mathcal{F}}$ . In this case, we give an explicit expression of the optimal dual node.

**Lemma 5** (Optimal dual node expression). The optimal dual node can be written as

$$\tilde{\mathbf{n}}_{\text{opt},c} = \frac{1}{\text{card}(F_c)} \sum_{i=1}^{\text{card}(F_c)} \mathbb{A}_i, \quad (67)$$

where  $\mathbb{A} := (\mathbb{P}_c^{\tilde{\mathcal{E}}})^T - |c|(\mathbb{P}_c^{\mathcal{F}})^+$  and the sum is over the set of columns of  $\mathbb{A}$ .

**Proof.** By definition  $\mathbb{R}_{\tilde{\mathbf{n}}_c}^{\mathcal{F}} = \frac{1}{|c|}(\mathbb{P}_c^{\tilde{\mathcal{E}}} - \mathbf{1}\tilde{\mathbf{n}}_c^T)^T$ . The objective function can be written as  $\frac{1}{|c|^2} \|\mathbb{A} - \tilde{\mathbf{n}}_c \mathbf{1}^T\|_2^2 = \frac{1}{|c|^2} \sum_i \|\mathbb{A}_i - \tilde{\mathbf{n}}_c\|_2^2$ , where the sum is over the set of columns of  $\mathbb{A}$ . By equating the gradient to zero we obtain the minimum point at  $\frac{1}{\text{card}(F_c)} \sum_i \mathbb{A}_i$ .  $\square$

## 6. Numerical results

We first verified the equivalence of the reconstruction operators introduced in [8] with the reconstructions operators defined by geometric elements of the dual barycentric grid in Section 5 by solving two multi-material patch tests on a grid made by general polyhedra. Then, a real-life stationary current conduction problem is solved using the geometric optimization of reconstruction operators described in Section 5.2. Finally, we show an example of the role of the dual barycentric dual grid for the correct computation of some global variables, in this case the current flowing through the electrodes.

The stationary current conduction is a Poisson problem in a connected region  $\Omega$  of the 3-D Euclidean space

$$\begin{aligned} \nabla \times \mathbf{E} &= \mathbf{0}, \\ \nabla \cdot \mathbf{J} &= 0, \\ \mathbf{J} &= \sigma \mathbf{E}, \end{aligned} \quad (68)$$

where  $\sigma$  is a material parameter called electric conductivity,  $\mathbf{E}$  and  $\mathbf{J}$  are the electric field and the current density vectors, respectively. The material parameter electric conductivity  $\sigma$  is assumed to be a positive scalar value which is piecewise uniform in each material region. The region boundary  $\partial\Omega$  is partitioned into a set of  $N^i$  surfaces of perfect insulators  $\partial\Omega_k^i$ , and a set of  $N^c + 1$  disjoint equipotential surfaces (*electrodes*) of perfect conductors  $\partial\Omega_k^c$ :

$$\partial\Omega = \sum_{k=1}^{N^i} \partial\Omega_k^i + \sum_{k=0}^{N^c} \partial\Omega_k^c. \quad (69)$$

Electrode  $\partial\Omega_0^c$  is considered as reference for all the voltages of the remaining electrodes, that are supposed to be assigned.  $\mathbf{J} \cdot \mathbf{n} = 0$  is set as boundary conditions (b.c.) on each  $\partial\Omega_k^i$ , where  $\mathbf{n}$  is the outwards oriented normal unit vector of  $\partial\Omega$ .

### 6.1. Multi-material patch tests

The multi-material patch tests are Poisson problems designed in such a way that their solution is piecewise-uniform. By interpreting the Poisson problems as direct current conduction problems, a simple way to produce multi-material patch test is to consider a resistor with two conductors with different material properties (called electric resistivity  $\rho$ ) placed in *series* or in *parallel* as described in detail later.

To test the edge mass matrices we use the classical scalar potential formulation *SP*. Instead, in order to test the face mass matrices we use the vector potential *VP* [27] or mixed-hybrid *MH* formulations [10], [28]. We remark that the *VP* and *MH* formulations produce the same results given that they are algebraically equivalent [28]. The polyhedral grid used

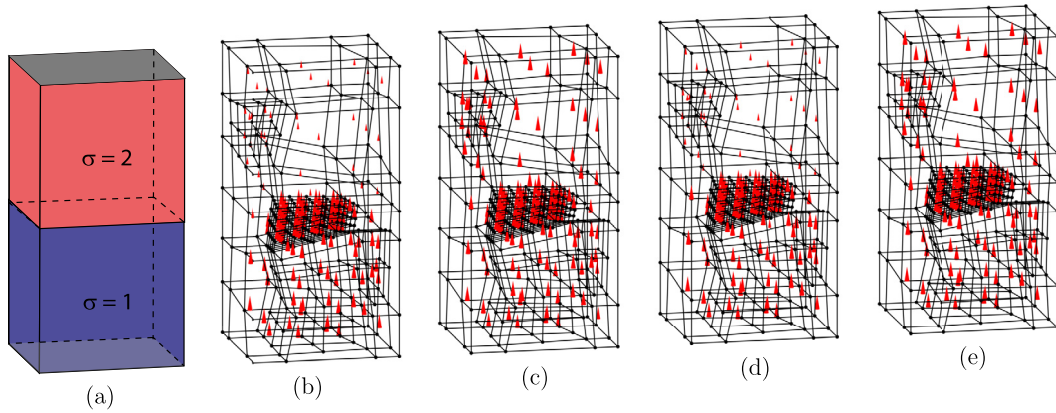


**Fig. 6.** The *series* multi-material patch test (a). We set the voltage between the two electrodes, represented in gray in the picture, to 1V. (b) Electric field  $\mathbf{E}$  produced by the *SP* formulation. (c) Current density field  $\mathbf{J}$  produced by the *SP* formulation. (d) Electric field  $\mathbf{E}$  produced by the *VP* formulation. (e) Current density field  $\mathbf{J}$  produced by the *VP* formulation.

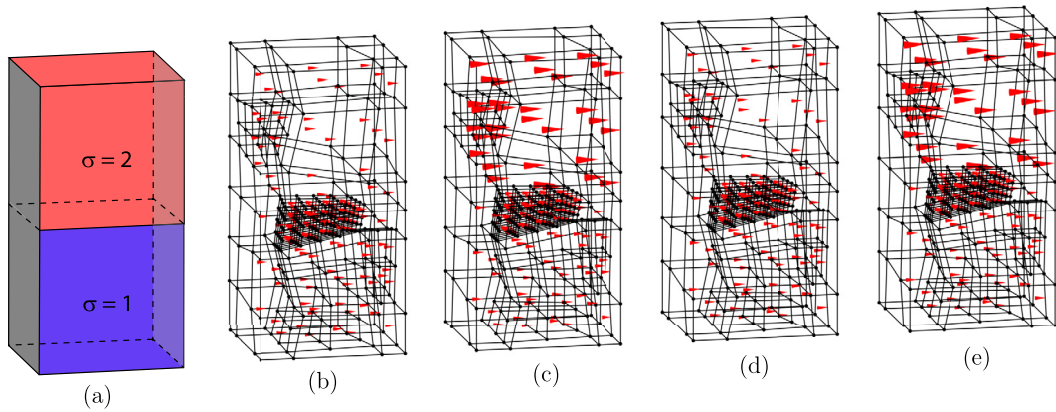


**Fig. 7.** The *parallel* multi-material patch test (a). We set the voltage between the two electrodes, represented in gray in the picture, to 1V. (b) Electric field  $\mathbf{E}$  produced by the *SP* formulation. (c) Current density field  $\mathbf{J}$  produced by the *SP* formulation. (d) Electric field  $\mathbf{E}$  produced by the *VP* formulation. (e) Current density field  $\mathbf{J}$  produced by the *VP* formulation.

in the example is formed by 131 nodes, 306 edges, 237 faces and 61 cells. The grid is obtained through two levels of sub-gridding of a few cells, so that the obtained elements are general polyhedra.

In the first multi-material patch test, two different materials with different material properties are placed in *series*. From the result represented in Fig. 6, we conclude that the tangential component of the electric field  $\mathbf{E}$  is conserved across the material interface, whereas the tangential component of the current density field  $\mathbf{J}$  jumps. This result holds for both formulations.

In the second multi-material patch test, two different materials with different material properties are placed in *parallel*. From the result represented in Fig. 7, we conclude that the normal component of the current density  $\mathbf{J}$  is conserved across the material interface, whereas the normal component of the electric field  $\mathbf{E}$  jumps. This result holds for both formulations.

## 6.2. Square resistor benchmark

As a more complicated example, we compute the conductance  $G$  of a square resistor [28], see Fig. 8. A voltage of  $u = 1$  V is enforced between the two electrodes, which are placed in the two lateral surfaces of the solid square torus. The conductor placed inside the solid torus has an electrical conductivity  $\sigma = 1$  S/m. This problem is interesting because, like most industrial problems, exhibits a singular analytical solution. Yet, the analytical solution is available and  $G = 10.23409256$  S. The conductance  $G$  is extracted by computing the total dissipated power  $P = G u^2 = \int_{\Omega} \frac{|\mathbf{J}|^2}{\sigma}$  or alternatively by using the Ohm's law  $G = i/u$ , where  $i$  is the current that flows between the two electrodes.

All simulations are performed using the optimal dual node for the geometric dual grid as described in Section 5.2. We do not observe a significant improvement in the convergence of the scheme although the reconstruction operator is locally optimized for every single cell. Here, the optimization is substantial for cells which are not symmetric. This can be qualitatively seen by the results of Section 5.2 where it is shown that where the cell is cubic the optimal dual node

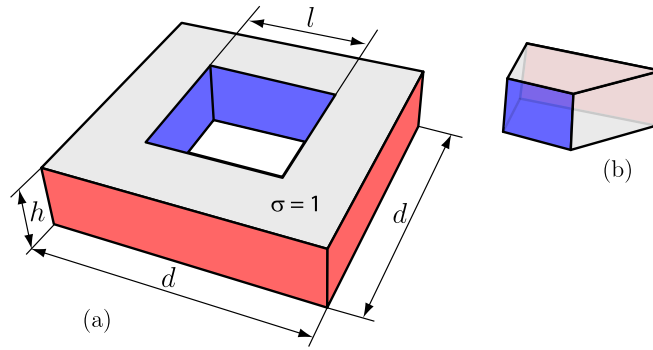


**Fig. 8.** (a) The geometry of the square resistor benchmark ( $h = 1$  m,  $d = 4$  m, and  $l = 2$  m). The two electrodes are depicted in red and blue. (b) Thanks to the symmetry, the computational domain has been reduced to one in eight of the resistor. (For interpretation of the colors in the figure(s), the reader is referred to the web version of this article.)

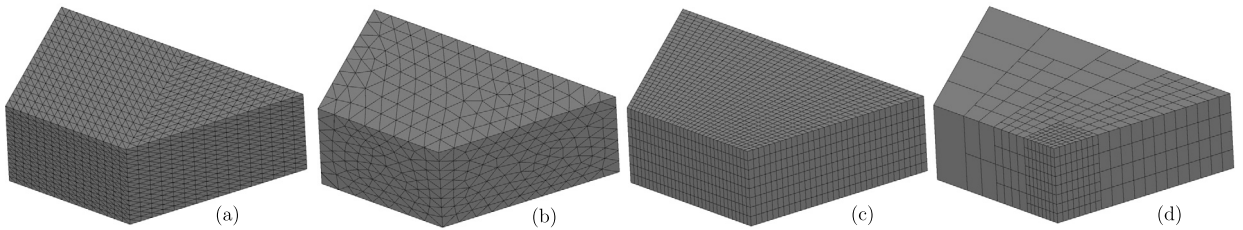


**Fig. 9.** The four different types of grids used to discretize the geometry of the square resistor in Fig. 8. (a) Structured tetrahedral grid. (b) Unstructured tetrahedral grid. (c) Structured hexahedral grid. (d) Polyhedral grid with *subgridding*.

coincides with the barycenter of the cell. We point out that the optimization can be performed as a preprocessing step that defines the optimal geometric structure of reconstruction operators.

The conductance of the square resistor has been evaluated by the *SP* and *VP = MH* formulations on refined grids. The results are collected in Fig. 10. First, it is interesting to note that the results relative to the scalar potential *SP* and to the vector potential *VP* or mixed-hybrid *MH* formulations provide, respectively, the upper and lower bounds for the conductance [29], [27]. This property is called *complementarity* in the computational electromagnetics community [28]. Second, in Fig. 9, four different types of grids have been used. Polyhedral grids with subgridding, i.e. a nonconforming-like local mesh refinement technique, appears to be particularly appealing.

A faster convergence can be reached only by using automatic mesh adaptivity. A comparison of the results obtained with tetrahedral and polyhedral unstructured meshes constructed with automatic mesh adaptivity is prevented by the lack of an automatic polyhedral mesh generator. Such a mesh generator is under development.

### 6.3. $P_0$ -consistent reconstruction operators and post-processing

Let us consider the problem described in the previous section 6.2. Now we show that the  $P_0$ -consistency property of reconstruction operators guarantees the continuous balance laws at the discrete level. To begin with, we observe that

$$\mathbf{CURL} \mathbf{E}^{\mathcal{C}} = \mathbf{0}, \quad (70)$$

so that an essential physical property of the continuous problem is preserved. What about the flux-conservation property of the discrete current density? The question naturally arises since in the mimetic framework DoFs of the current density  $\mathbf{J}$  are not explicitly defined. As a first approach to assess the discrete conservation property of  $\mathbf{J}$ , let  $\mathbf{E}_r$  be the cell-wise electric field reconstructed starting from edge DoFs. Then, we denote by  $\mathbf{J}_r$  the *reconstructed* current density defined on each cell multiplying  $\mathbf{E}_r$  by the corresponding conductivity, assumed to be constant over each cell. Although  $\mathbf{J}_r$  is divergence-free inside cells, there are flux “leaks” between faces of the primal grid. To validate this assertion, let  $I_1$  and  $I_2$  be the inward and outward current of  $\mathbf{J}_r$  through the two pair of electrodes  $\partial\Omega_1^{\mathcal{C}}$  and  $\partial\Omega_2^{\mathcal{C}}$ , respectively. For the problem under consideration, the following values are found  $I_1 = 1.3830$  and  $I_2 = 1.0916$ . Thus, the computed currents are “non-physical” since an essential physical property is violated, namely the fact that  $I_1$  have to be equal to  $I_2$ . Thus,  $I_1$  and  $I_2$  do not represent a good approximation of the current through the resistor.

On the contrary, compute accurately the current through the electrodes is very important in many applications like Electrical Impedance Tomography (EIT). The results of Section 4 shed light on the reasons why one should not integrate the reconstructed current density  $\mathbf{J}_r$  on faces on the primal grid. Indeed, by requiring  $\widehat{\mathcal{DIV}} \mathbf{E}^{\mathcal{C}} = \mathbf{0}$ , we obtain

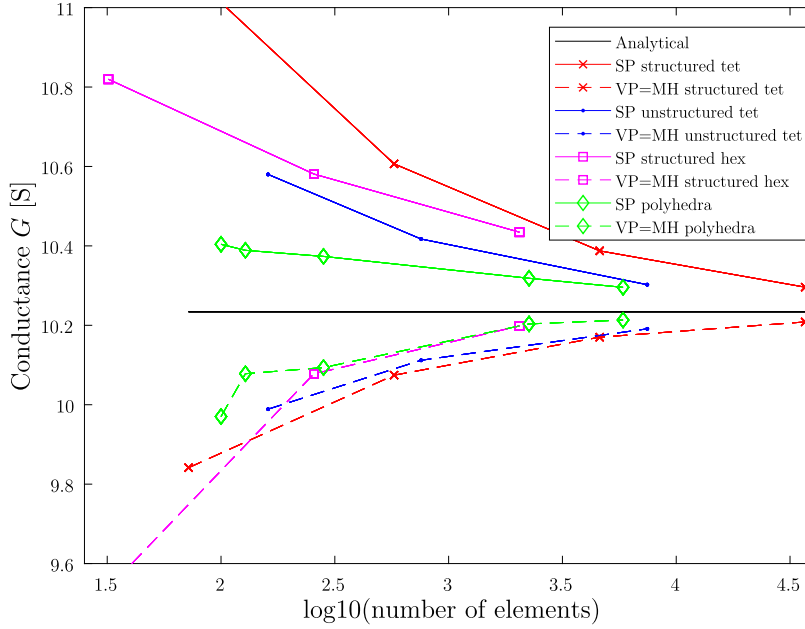


Fig. 10. Results for the square resistor benchmark.

$$\text{row}_n \mathbb{G}^T \left( \sum_{c \in \mathcal{C}} (\mathbb{S}_c^{\mathcal{E}})^T |c| (\mathbb{R}_c^{\mathcal{E}})^T \mathbf{J}_{r,c} \right) = 0, \forall n \in N, n \notin \partial \Omega. \tag{71}$$

So discrete solenoidality requires that the flux of  $\mathbf{J}_r$  through the geometric closed surface associated with  $P_0$ -consistent edge reconstructions operators of every inner node vanishes. Therefore, we may aggregate geometric closed surfaces associated with inner nodes, and the flux of  $\mathbf{J}_r$  will vanish across such an aggregate. Based on these results, let us compute the following quantity

$$I_1 = \sum_{n \in \partial \Omega_i^c} \text{row}_n \mathbb{G}^T \left( \sum_{c \in \mathcal{C}} (\mathbb{S}_c^{\mathcal{E}})^T |c| (\mathbb{R}_c^{\mathcal{E}})^T \mathbf{J}_{r,c} \right) \tag{72}$$

as the discrete approximation of the current of  $\mathbf{J}$  through  $\partial \Omega_i^c$ , where a similar expression holds for  $I_2$ . Then, we see that

$$\sum_{n \in N} \text{row}_n \mathbb{G}^T \left( \sum_{c \in \mathcal{C}} (\mathbb{S}_c^{\mathcal{E}})^T |c| (\mathbb{R}_c^{\mathcal{E}})^T \mathbf{J}_{r,c} \right) = 0 = I_1 + I_2, \tag{73}$$

where we have used the given boundary values of  $\mathbf{J}$ . Thus, we have  $I_1 = -I_2 = 1.3225$ , proving the physical soundness of the computed quantities (up to a minus sign, which accounts for the orientation of the surfaces).

Another remarkable result is that the obtained current  $I_1 = -I_2$  coincides up to machine precision with the dissipated power inside the resistor computed in previous section as  $P = G u^2 = \int_{\Omega} \frac{|\mathbf{J}|^2}{\sigma}$  (given that  $u$  is fixed to 1V with boundary conditions).

As shown in Section 5, a canonical way of constructing  $P_0$ -consistent reconstruction operators is given by barycentric dual grid. In this case, (72) can be interpreted as the sum of currents through dual faces. We point out that the current in (72) is equal through every homologous surface associated with a different choice of the  $P_0$ -consistent edge reconstruction operators.

### 7. Conclusions

In this paper, we have studied hidden geometric aspects of low-order compatible numerical schemes for arbitrary polyhedral grids. First, we have shown that standard mimetic numerical schemes have noteworthy geometric properties. These geometric properties were demonstrated by reformulating standard mimetic reconstruction operators using geometric elements of the barycentric dual grid, thus proving the equivalence between mimetic and geometric approaches. Second, we have introduced the class of  $P_0$ -consistency reconstruction operators which extends the standard consistency requirement of the mimetic framework. A characterization of these operators is given as an affine solution space of a linear system of equations. Given the geometric description of the scheme, this analysis reveals the existence of many dual grids that define reconstruction operators and constitutes the starting point to optimize them. Additionally, it shows that the barycentric dual

grid is a canonical way of designing  $P_0$ -consistency reconstruction operators at single element level. The fundamental role played by Stokes theorem in mimetic numerical schemes appears, therefore, as the geometric manifestation of the necessity of using the barycentric dual grid to design local reconstruction operators. Numerical examples show the importance of the geometric interpretation for the correct evaluation of some physical variables in the post-processing stage, thus motivating the practical impact of including them as part of the numerical scheme.

### CRediT authorship contribution statement

Silvano Pitassi: Conceptualization, Methodology, Writing- Original draft preparation.  
 Francesco Trevisan: Conceptualization, Writing - Review & Editing Ruben Specogna: Conceptualization, Methodology, Supervision, Writing- Reviewing and Editing, Software.  
 Riccardo Ghiloni: Supervision, Writing - Review & Editing.

### Declaration of competing interest

The authors declare that they have no known competing financial interests or personal relationships that could have appeared to influence the work reported in this paper.

### References

- [1] E. Tonti, *On the Formal Structure of Physical Theories*, Monograph of the Italian National Research Council, 1975.
- [2] T. Tarhasaari, L. Kettunen, A. Bossavit, Some realizations of a discrete Hodge operator: a reinterpretation of finite element techniques [for em field analysis], *IEEE Trans. Magn.* 35 (1999) 1494–1497.
- [3] E. Tonti, The mathematical structure of classical and relativistic physics. A general classification diagram, <https://doi.org/10.1007/978-1-4614-7422-7>, 2013.
- [4] J. Munkres, *Elements of Algebraic Topology*, Perseus Books, Cambridge, MA, 1984.
- [5] C. Mattiussi, An analysis of finite volume, finite element and finite difference methods using some concepts from algebraic topology, *J. Comput. Phys.* 133 (1997) 289–309.
- [6] R. Hiptmair, Discrete Hodge-operators: an algebraic perspective, *Prog. Electromagn. Res.* 32 (2001) 247–269.
- [7] A. Bossavit, *Computational Electromagnetism*, Academic Press, 1998.
- [8] K. Lipnikov, G. Manzini, M. Shashkov, Mimetic finite difference method, *J. Comput. Phys.* 257 (2014) 1163–1227.
- [9] O. Zienkiewicz, R. Taylor, The finite element patch test revisited a computer test for convergence, validation and error estimates, *Comput. Methods Appl. Mech. Eng.* 149 (1997) 223–254. Containing papers presented at the Symposium on Advances in Computational Mechanics.
- [10] F. Brezzi, K. Lipnikov, V. Simoncini, A family of mimetic finite difference methods on polygonal and polyhedral meshes, *Math. Models Methods Appl. Sci.* 15 (2005) 1533–1551.
- [11] J. Bonelle, D.A. Di Pietro, A. Ern, Low-order reconstruction operators on polyhedral meshes: application to compatible discrete operator schemes, *Comput. Aided Geom. Des.* 35–36 (2015) 27–41.
- [12] L. Codecasa, R. Specogna, F. Trevisan, Symmetric positive-definite constitutive matrices for discrete eddy-current problems, *IEEE Trans. Magn.* 43 (2007) 510–515.
- [13] L. Codecasa, R. Specogna, F. Trevisan, Base functions and discrete constitutive relations for staggered polyhedral grids, *Comput. Methods Appl. Mech. Eng.* 198 (2009) 1117–1123.
- [14] L. Codecasa, R. Specogna, F. Trevisan, A new set of basis functions for the discrete geometric approach, *J. Comput. Phys.* 229 (2010) 7401–7410.
- [15] E. Tonti, A direct discrete formulation of field laws: the cell method, *Comput. Model. Eng. Sci.* 2 (2001) 237–258.
- [16] E. Tonti, Finite formulation of the electromagnetic field, *Prog. Electromagn. Res.* 32 (2001) 1–44.
- [17] A. Bossavit, Generalized finite differences in computational electromagnetics, *Prog. Electromagn. Res.* 32 (2001) 45–64.
- [18] A. Palha, P.P. Rebelo, R. Hiemstra, J. Kreeft, M. Gerritsma, Physics-compatible discretization techniques on single and dual grids, with application to the Poisson equation of volume forms, *J. Comput. Phys.* 257 (2014) 1394–1422. Physics-compatible numerical methods.
- [19] J. Bonelle, A. Ern, Analysis of compatible discrete operator schemes for elliptic problems on polyhedral meshes, *ESAIM: Math. Model. Numer. Anal.* 48 (2014) 553–581.
- [20] J. Droniou, R. Eymard, T. Gallouët, R. Herbin, A unified approach to mimetic finite difference, hybrid finite volume and mixed finite volume methods, *Math. Models Methods Appl. Sci.* 20 (2010) 265–295.
- [21] K. Lipnikov, G. Manzini, A high-order mimetic method on unstructured polyhedral meshes for the diffusion equation, *J. Comput. Phys.* 272 (2014) 360–385.
- [22] D.A.D. Pietro, J. Droniou, F. Rapetti, Fully discrete polynomial de Rham sequences of arbitrary degree on polygons and polyhedra, *Math. Models Methods Appl. Sci.* (2020) 1–47.
- [23] F. Brezzi, A. Buffa, G. Manzini, Mimetic scalar products of discrete differential forms, *J. Comput. Phys.* 257 (2014) 1228–1259.
- [24] F.J. Branin, The algebraic-topological basis for network analogies and the vector calculus, in: *Proceedings of the Symposium on Generalized Networks*, vol. 16, Polytechnic Institute of Brooklyn, 1966, pp. 453–491.
- [25] M. Marrone, Properties of constitutive matrices for electrostatic and magnetostatic problems, *IEEE Trans. Magn.* 40 (2004) 1516–1520.
- [26] S.L. Campbell, C.D. Meyer, *Generalized Inverses of Linear Transformations*, Society for Industrial and Applied Mathematics, 2009.
- [27] R. Specogna, Complementary geometric formulations for electrostatics, *Int. J. Numer. Methods Eng.* 86 (2011) 1041–1068.
- [28] R. Specogna, One stroke complementarity for Poisson-like problems, *IEEE Trans. Magn.* 51 (2015) 1–4.
- [29] J. Synge, *The Hypercircle in Mathematical Physics: A Method for the Approximate Solution of Boundary Value Problems*, Cambridge Univ. Press, NY, 1957.